Implementation and Validation of 3-D Ice Accretion Measurement Methodology

Sam Lee[*]
Vantage Partners, LLC, Cleveland, OH, 44135

Andy P. Broeren,[†] Richard E. Kreeger,[‡] and Mark Potapczuk[§]
NASA Glenn Research Center, Cleveland, OH, 44135

and

Lloyd Utt[**]
University of Akron, Akron, OH, 44242

A research program has been implemented to develop and validate the use of a commercial 3-D laser scanning system to record ice accretion geometry in the NASA Icing Research Tunnel. A main component of the program was the geometric assessment of the 3-D laser scanning system on a 2-D (straight wing) and a 3-D (swept wing) airfoil geometries. This exercise consisted of comparison of scanned ice accretion to castings of the same ice accretion. The scan data were also used to create rapid prototype artificial ice shapes that were scanned and compared to the original ice accretion.

The results from geometric comparisons on the straight wing showed that the ice shape models generated through the scan/rapid prototype process compared reasonably well with the cast shapes. Similar results were obtained with the geometric comparisons on the swept wing. It was difficult to precisely compare the scans of the cast shapes to the original ice accretion scans because the cast shapes appear to have shrunk during the mold/casting process by as much as 0.10-inch. However the comparison of the local ice-shape features were possible and produced better results. The rapid prototype manufacturing process was shown to reproduce the original ice accretion scan normally within 0.01-inch.

Nomenclature

CAD	=	Computer aided design
CT	=	Computed tomography
IRT	=	Icing Research Tunnel
LWC	=	Liquid water content
MVD	=	Median volumetric diameter
RPM	=	Rapid prototype manufacturing
SLA	=	Stereolithography
T_0	=	Total air temperature
t	=	Icing spray time
V	=	Tunnel airspeed
α	=	Angle of attack
Λ	=	Wing sweep angle

[*] Engineer IV, Icing Branch, 21000 Brookpark Rd., MS 11-2, AIAA Senior Member.
[†] Aerospace Engineer, Icing Branch, 21000 Brookpark Rd., MS 11-2, AIAA Associate Fellow.
[‡] Aerospace Engineer, Icing Branch, 21000 Brookpark Rd., MS 11-2, AIAA Associate Fellow.
[§] Aerospace Engineer, Icing Branch, 21000 Brookpark Rd., MS 11-2, AIAA Senior Member.
[**] Student, Dept. of Mechanical Engineering, Auburn Science and Engineering Center (ASEC) 101.

I. Introduction

The chief product of an icing wind tunnel is the ice accretion that forms on a wide variety of test articles such as airplane wings, rotor blades, engine inlets, radomes and other flight hardware. The shapes are often used for the following: follow-on computational or experimental aerodynamic studies, development of design criteria or requirements, and engineering tool development, improvement or validation. Broeren et al.[1] describe a recently completed comprehensive study of aerodynamic simulation of ice accretion. For some cases such as initial roughness, spanwise ridges and streamwise type ice shapes, the fine geometric details can be important to the resulting aerodynamics. Therefore, documentation of the resulting ice accretion is a key piece of data in icing-wind-tunnel tests.

There are a number of currently used options for documenting ice accretion in icing-wind-tunnel testing. They range from simple photographs and pencil tracings to mold and casting methods. The most commonly used method is the cross-sectional tracing, which does not capture three-dimensional features of ice accretion. The best technology to-date for capturing three-dimensional features of ice accretion is the mold and casting method.[2] The mold and casting method has limitations in utility since it is not easily scaled or translated into a digital form. If a method to accurately and efficiently digitize ice accretion in three dimensions was available, not only would documenting ice accretion in tunnel testing be improved (particularly for capturing three-dimensional features), but utility of use of that information for other research purposes would be increased. Laser-based and other optical scanning methods have been investigated to accomplish three-dimensional digitization of ice accretion. Given recent advances in technology and the motivations described earlier, NASA has incorporated development of three-dimensional ice accretion digitization methods into its research plans.

The main goal of the Airframe Icing Technical Challenge of the Atmospheric Environment Safety Technologies Project of the NASA Aviation Safety Program is to achieve acceptance of experimental and computational icing simulation tools in super-cooled large droplet (SLD) conditions and on three-dimensional airframe components, including swept wings.[3,4] Since this goal focuses on three-dimensional geometries, it was necessary to develop a suitable means of recording and archiving fully three-dimensional descriptions of experimental ice accretion geometry. A research plan to develop this capability was introduced in the NASA Aviation Safety Program Technical Meeting in 2011.[5] This research was divided into two phases. The first phase considered selection of a laser-scanning system and software. This has been completed and the results were described in Lee et al.[6] The second phase considered validation of the system and a declaration of capability for use in future icing experiments. These results are described in this paper. The system has since been used in icing tests at NASA.[7,8]

The roadmap of Phase I is shown in Fig. 1. There were numerous commercial 3-D laser scanning systems and post-processing software available in the market. It was necessary to develop a process to identify the most appropriate system for purchase and further development. Parallel plans were developed to identify the most suitable scanner hardware and software systems.

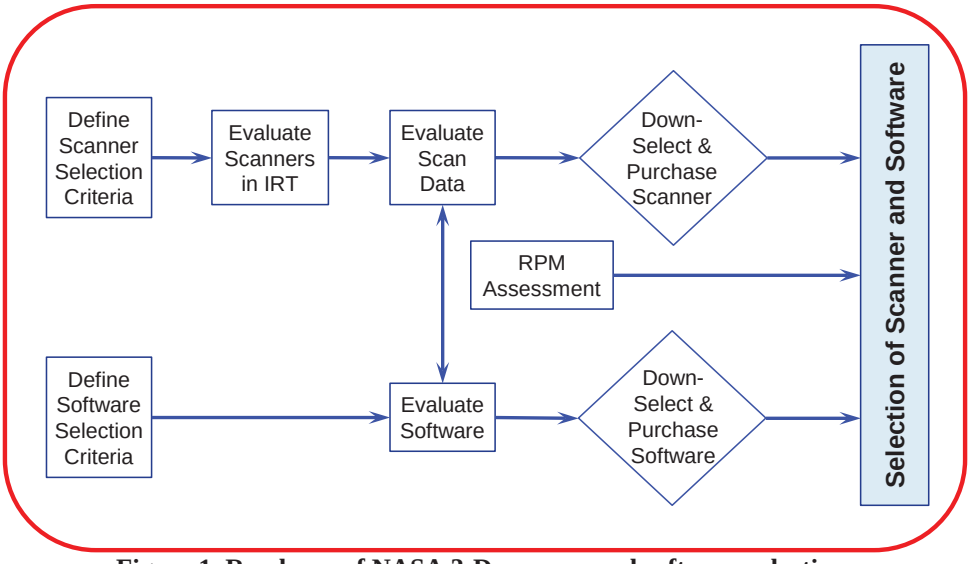

Figure 1 Roadmap of NASA 3-D scanner and software selection.

The first task in the plan was to define the criteria that were used to evaluate the scanner hardware and software. The hardware selection criteria were based on the ability of the scanner to operate in the IRT test section environment under a wide range of temperature and humidity conditions and the ability of the system to scan various types of ice accretion. The software selection criteria were based on the compatibility of the software with various scanners that were evaluated and the ability to process the data effectively and efficiently.

Several scanner manufacturers were invited to demonstrate the capability of their scanners in the IRT test section environment. The evaluation procedure was established such that the scanners were judged against the selection criteria. Identical evaluation processes were used when possible, and the scanners were operated in a wide range of tunnel conditions and scanned a wide range of ice shape types. The results of the IRT scanner evaluation and software evaluation were used to identify the most capable and promising system for further development. Also included in Phase I was the assessment of the current rapid prototype methods that can be used to manufacture the ice shapes from the 3-D scan data.

The results of Phase I showed that commercial 3-D laser scanners were capable of recording many details of various types of ice shapes, and post-processing software were capable of generating "water-tight" surfaces. The scanners that were evaluated in the IRT had similar abilities to digitize ice shapes because the scanning methods were identical. The primary differences were the method that each system used to position the scanner and the ability to operate in the IRT test section environment. Several scanning systems (hardware and software) were evaluated against selection criteria, and the Romer Absolute SI scanner[9] and Geomagic Studio software[10] were found to be the most promising. This scanning system was purchased by NASA and was used to implement and validate the use of this technology through a series of icing and aerodynamic tunnel tests.

Phase II was built on the methodology developed by Broughton[11] during the previous attempt at developing a 3-D scanning capability for the IRT, but it was be greatly expanded upon. The roadmap of this portion of the project is shown in Fig. 2. The implementation tasks involved developing procedures for using the scanner in the IRT as well as for post-processing the data.

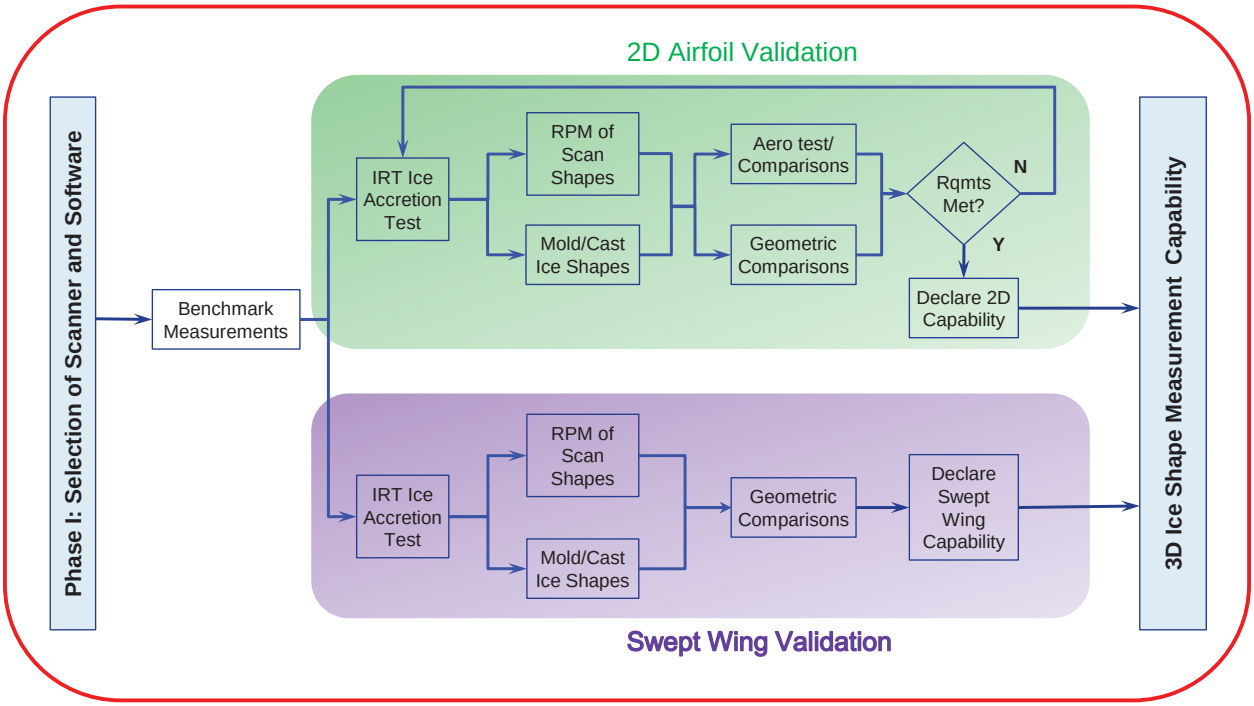

Figure 2 Roadmap of NASA 3-D ice shape measurement implementation and validation project.

The first component in the Phase II of the research was an exercise to help benchmark the measurement capability of the scanning system that was identified and purchased during Phase I. These benchmark measurements were performed on a metal "roughness sample" block using the methodology established by Broughton.[11]

The main component of the validation (as shown in the top leg of the roadmap in Fig. 2) was the "circular" geometric and aerodynamic assessment on a 2-D (straight wing) airfoil geometry. This exercise consisted of comparison of scanned ice shapes to castings of the same ice shape (up to this point the only means of recording

fully three dimensional ice shapes). The scan data were also used to create RPM artificial shapes that were scanned and compared to the original ice accretion. A closely related aerodynamic evaluation was also to be conducted, where RPM artificial shapes made from ice scans were compared against ice-shape castings in an aerodynamic wind tunnel. These validations (both geometric and aerodynamic) were conducted for each of the four basic categories of ice accretion as identified by Broeren et al[1]: glaze horn, roughness, rime (streamwise) and runback (spanwise ridge).

The third component was a geometric validation that was performed on a 3-D, swept-wing geometry (as shown in the bottom leg of the roadmap in Fig. 2). This was specifically intended to quantify the limitations of capturing very complicated scallop geometries and develop methods to ameliorate these limitations. The swept wing validation did not contain an aerodynamic assessment.

This paper describes the results of the Phase II implementation and validation portion of the 3-D scanner development effort at NASA. It describes the procedures used in the IRT tests to generate the validation data as well methods used to process the data and manufacture the RPM models used for aerodynamic and geometric validation. The results of geometric validation (from both benchmark measurements and ice shapes) are presented as well. The detailed results of the aerodynamic validation on a 2-D airfoil section are presented in Broeren et al.[12]

II. Ice Shape Scanning Procedure

The two airfoil models used for this study were a full-span, 18-inch chord NACA 23012 (2-D airfoil validation) and a semi-span 36-inch chord NACA 0012 model (swept wing validation) that could be swept at 30 and 45 deg. Both of the models were equipped with a removable leading edge. They were mounted vertically in the test section on a turntable, as shown in Fig. 3.

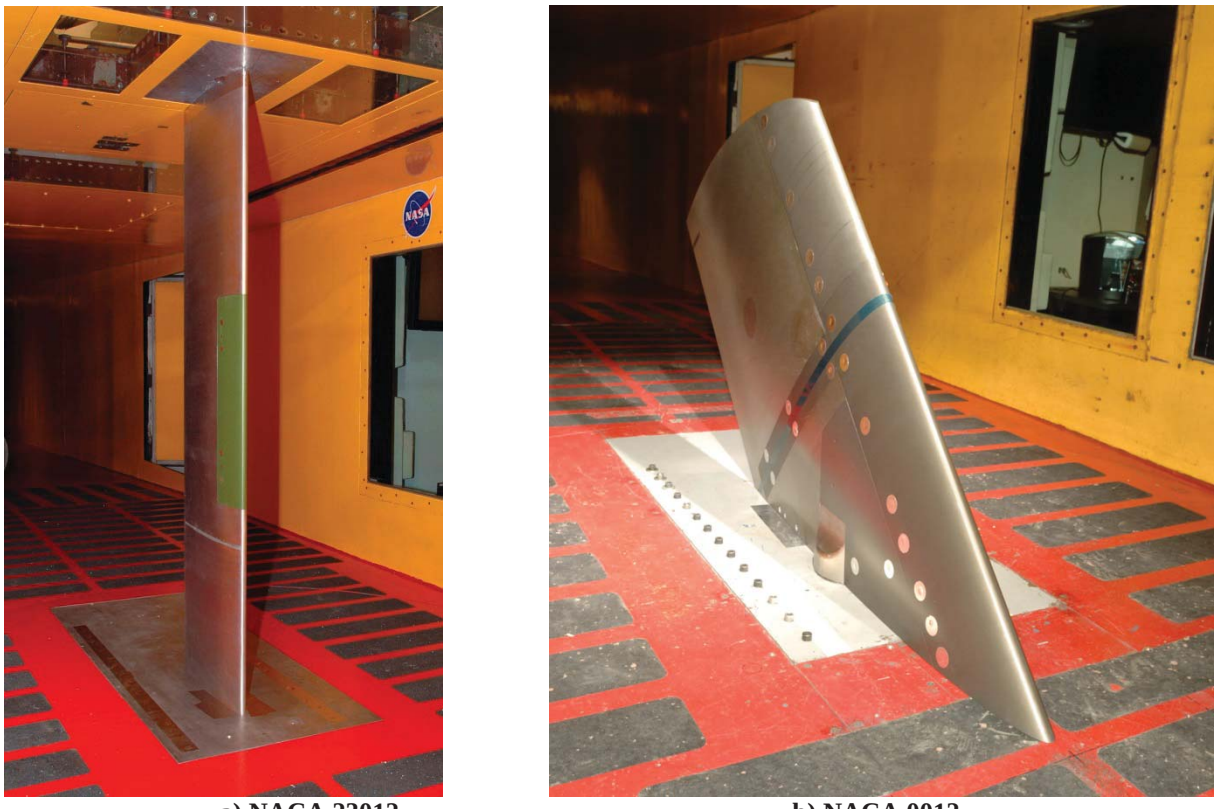

a) NACA 23012 **b) NACA 0012**

Figure 3 Airfoil models used in this study.

The 3-D scanner used for this study was a Romer 7520SI articulating arm with an integrated laser scanner (Fig. 4). The laser scan head was mounted on the end of a 7-axis arm. The operator positioned the scan head manually,

and the absolute encoders built into the arm tracked the location of the scanner head relative to the base of the arm. The scan data were referenced to the location of the base of the arm. The arm was constructed of thermally stable carbon fiber and did not require any thermal compensation. It had a measurement reach of 6 ft. The scanner projected a scan line 2.3-in wide, with a maximum resolution of 0.002 in. The system operated at 30 Hz (i.e. one scan line every 0.03 seconds). The maximum resolution in the direction of the scanner movement was limited by the speed the operator could smoothly move the arm (typically not less than 0.50 in/sec, resulting in a resolution of 0.015 in). Because of this, it had a much higher resolution in the direction of the laser scan line than in the direction of the scan. The Romer scanner was operated directly from Geomagic through a plug-in. The data was acquired through a combination of USB and Ethernet ports. The scanner was also fitted with a hard-probe for tactile-based, single-point measurements that was used to capture model reference points and planes. A more detailed description of how laser scanners operate and their limitations is described in Lee et al.[6]

Figure 4 Romer scanner used for this study.

The base of the scanner was mounted on top of a 22-inch tall aluminum riser tube in order to provide extra height and reach. The riser tube in turn was attached to a steel plate using magnetic locks. The steel plate was bolted to the tunnel turntable. The steel plate was required to provide a flat, ferrous surface for the magnetic locks. The scanner setup for the tests is shown in Fig. 5. For the validation tests on the straight airfoil model, the scanner was mounted upstream of the airfoil model, as shown in Fig 5a. For the swept wing tests, the scanner was mounted the on the lower surface side of the model (Fig. 5b). The two different sweep angles (30 and 45 deg) required two different scanner locations.

a) Scanner setup for straight-wing tests

b) Scanner setup for swept-wing tests

Figure 5 Scanner setup

Both of the models were originally built without any reference points for the scanner, since they were constructed prior to the use of the scanner. When the leading edge of the model was removed, there were internal planes (Fig. 6a) that could be probed and used as geometric reference. Five internal planes were available on the straight wing model, and four internal planes were available on the swept wing model. Five reference points (consisting of counter-sunk holes) were drilled into the surface of the model. These points were identified using the hard-probe attachment along with the reference planes, as shown in Fig. 6b. These were used to obtain an airfoil model-based coordinate system which will be explained in more detail later in the paper. The probing measurements were all taken around 20 deg F in order to minimize the thermal-induced geometric differences in the model between when the reference points were taken and when the ice accretion scans were taken.

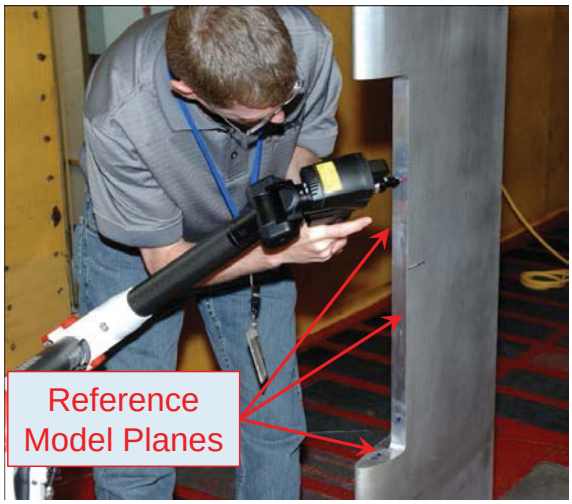

a) Probing reference planes

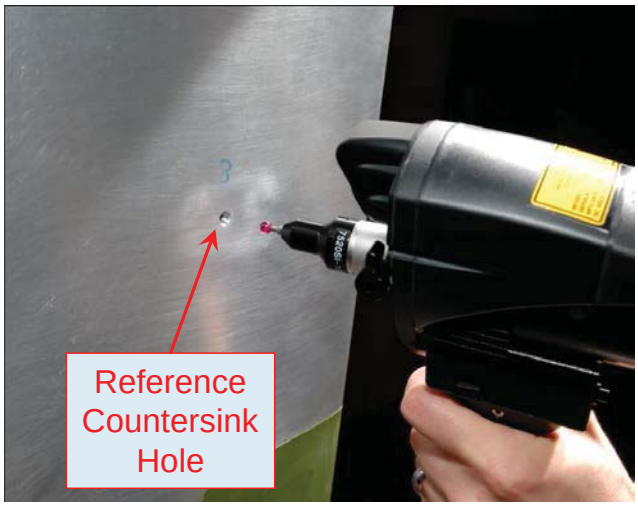

b) Probing reference point

Figure 6 Obtaining reference locations on the straight wing model.

The IRT scanner test procedure consisted of the following six steps:

1. Accrete ice on the test article
2. Photograph the ice
3. Spray the ice with white paint
4. Install and set up the scanner

5. Scan the ice accretion
6. Make molds of the ice accretion

After the ice was accreted on the model, it was coated with highly-reflective, diffuse, white paint. The paint mixture was comprised of the following materials in the proportions listed:

- 20g TiO_2 pigment
- 20g Poly(2,6-dimethyl-1,4-phenylene oxide) binder
- 500ml Tetrahydrofuran solvent

The mixture was blended using an ultrasonic mixer and applied on the ice using an automotive-style spray gun as shown in Fig. 7. After the ice was painted, the scanner and the laptop computer to control the scanner were brought into the test section.

The ice was scanned until a sufficient level of detail had been captured over the airfoil model in the center 1.5 ft. section of the test section (Fig. 8). The operator scanned the ice accretion using straight smooth passes, going as slowly as possible while still maintaining smooth motion. As stated before, the scanner resolution in the direction of the scan was determined by the speed the scanner was moved, so the highest resolution was obtained by moving the scanner as slow as possible. Because the scanner had a much higher resolution in the direction of the laser line than in the direction of the scan, another scan pass perpendicular to the direction of previous scan was required if finer ice accretion details like roughness was needed. It was also important to have an overlap region of 1/3 the scan line width between adjacent scan passes in order to align or register the scans. The final step in the scanning procedure was to acquire the hard probe points of the five reference holes for future alignment to the airfoil model-based coordinate system.

After the scan was completed, the scanner and the computer were removed from the tunnel test section. The removable leading edge was then removed and placed in a mold box in order to make a mold of the ice accretion. The casting of the ice accretion was made from the mold as described in detail by Monastero.[13]

Figure 7 Painting ice accretion.

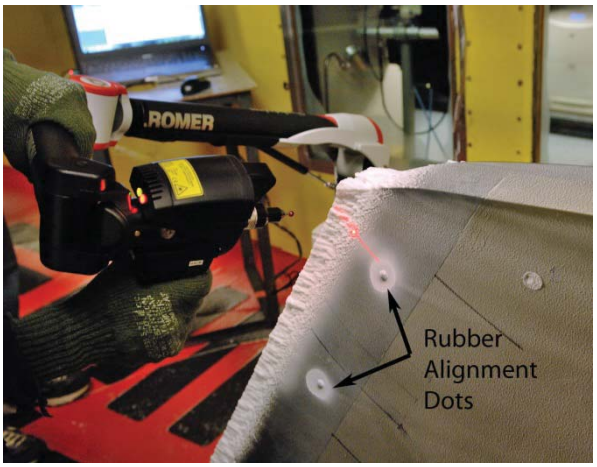

Figure 8 Scanning ice accretion.

III. Scan Data Processing Procedure

The ice accretion scan data were processed into water-tight surfaces using Geomagic Studio. The straight-wing ice scans were then turned into artificial leading-edge ice shapes for testing on an 18-in chord NACA 20312 airfoil model in the University of Illinois aerodynamic wind tunnel. They were constructed using both stereo lithography (SLA) and High Density PolyJet rapid-prototype manufacturing methods. They were instrumented with surface pressure taps that were incorporated into the 3-D CAD models used to manufacture the shapes. Artificial ice-shape leading edges were also constructed using the traditional mold/casting methods for both geometric and aerodynamic

comparisons. The results and analysis of the geometric comparison between the RPM shapes and the cast shapes are included in this paper. The results of the aerodynamic comparison between the RPM shapes and the cast shapes are included in the companion paper by Broeren et al.[12]

The methods used for processing raw ice accretion scan data into a water-tight 3-D mesh for documentation and rapid prototype manufacturing for aerodynamic testing are described in this section. These methods were used to process data acquired with a Romer Absolute scanner using Geomagic software. Other scanner/software combinations may require significantly different procedures.

Each scanned ice accretion was comprised of multiple ordered point cloud objects. Each pass of the scanner resulted in an ordered point-cloud object. An ordered point cloud is one that already has the points in a uniformly-spaced rectangular grid pattern, as shown in Fig. 9. The green surface shown in the figure is displayed by Geomagic only as a visual aid. At this point, the scan data do not have surfaces. Typically 20 to 40 scan passes were required to capture a single ice shape.

Figure 9 Ordered scan data points.

A. Registration Alignment

The first step in processing the scan data was to align the scan objects using the Global Registration feature within Geomagic Studio. Global Registration reoriented the scan objects so that the common or shared regions coincided. Due to the uncertainties in the scanner, there was usually a slight offset in the overlap regions of the scan objects, usually between 0.001-in to 0.003 -in. This is illustrated in Fig. 10a, which shows the individual scan objects in different color. This particular ice shape scan consisted of 30 scan objects. There are distinct color regions with very little bleed-through or blending of colors, indicating that there was an offset in the overlap regions of the scan objects. Global Registration aligned the scan objects by applying "best-fit" in the overlap regions using an iterative process. The result is shown in Fig. 10b, where there is now bleeding or blending of colors in the overlap regions of the scan objects, indicating a very good alignment.

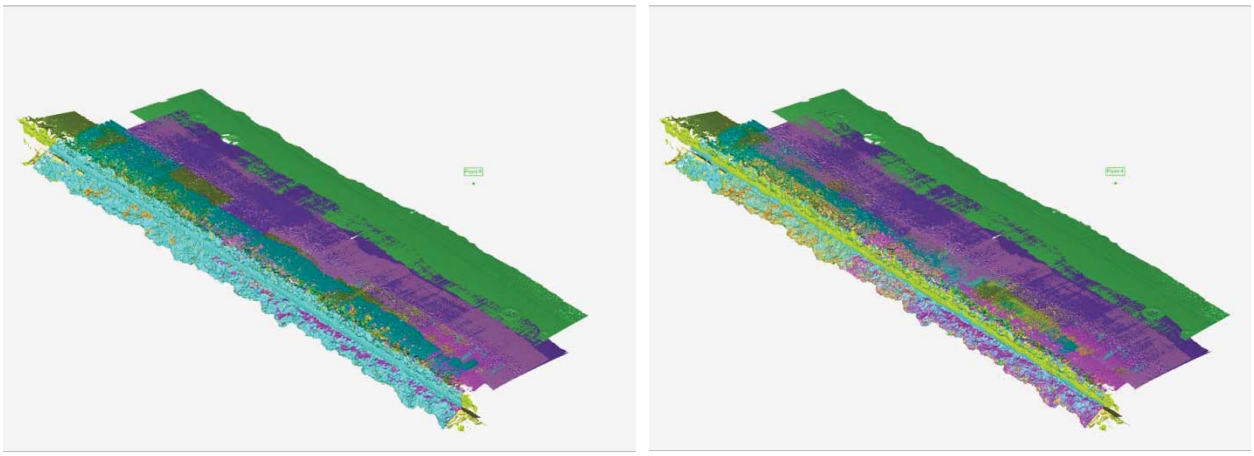

a) Prior to global registration **b) After global registration.**

Figure 10 Scan objects prior and after global registration

B. Combining Point Objects/Reduce Points

The next step in the data processing procedure was to combine the numerous point-scan objects that made up the ice accretion scan into a single point cloud object and reduce the number of data points. This was done through the Combine Point Object function within Geomagic Studio. This process also removed all of the overlap regions and usually decreased the number of points by 20-30%. Before a surface wrap can be applied to the data set, the number of points needed to be reduced further. At this point, there were usually 10-20 million data points, and it was desirable to reduce the point cloud to 1 to 1.5 million points. With the current capabilities of the desktop computing, a wrapped surface from a larger data set of points cannot be processed further with any reasonable efficiency.

C. Water-Tight Wrap

The point cloud data were converted to a triangular surface mesh (constructed of connected triangles) using the Wrap feature within Geomagic Studio. The number of triangles in the surface mesh was double the number of points in the point cloud, and was usually kept below 3 million. It was very difficult and time consuming to work with a larger number of triangles with the current generation of computers, so meshes with a large number of triangles were not generated.

The Wrap process resulted in varying number and size of holes, depending on the types of ice accretion. One of the chief limitations of the laser-based scanners is that it is based on line of sight. The camera on the scanner is offset from the laser (typically by 30 deg.), so if the camera cannot "see" the projected laser line on the surface, it cannot scan. This usually occurs on features that exceed a certain depth or are shadowed by other ice features. The holes were regions of ice shape that the scanner could not scan. Roughness and rime ice accretion resulted in the smallest holes, and complex shapes such as swept-wing scallop ice resulted in the largest holes, as shown in Figs. 11 and 12. Fig 11a shows a roughness ice shape immediately after the Wrap step. The holes are shown by regions bounded by green lines. The outer surface of the scan is shown in blue, and the inner surface of the scan is shown in yellow. It shows that the roughness ice resulted in a few small holes that that could quickly and easily be filled into a water-tight surface shown in Fig 11b. Figure 12a shows a scallop ice immediately after the Wrap step, showing numerous large holes. It took significantly more time and effort to convert the scan into the water-tight surface shown in Fig. 12b. The roughness ice shown in Fig. 11 took 10 minutes to turn into a watertight surface using mostly automated features of Geomagic, while the scallop ice shown in Fig.12 took 5 hours using mostly manual tools. The next section describes the procedure used fill in the mesh holes.

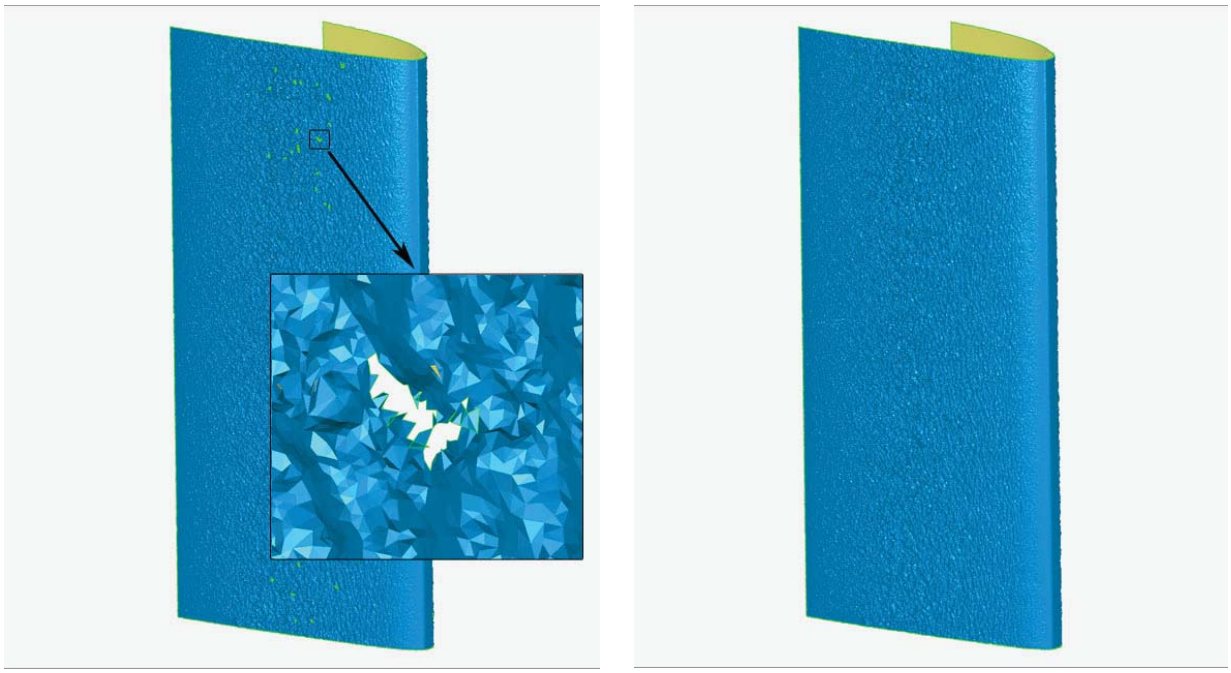

a) Mesh holes after Wrap function **b) Mesh after made water-tight.**

Figure 11 Roughness ice immediately after meshing and after processed into water tight surface.

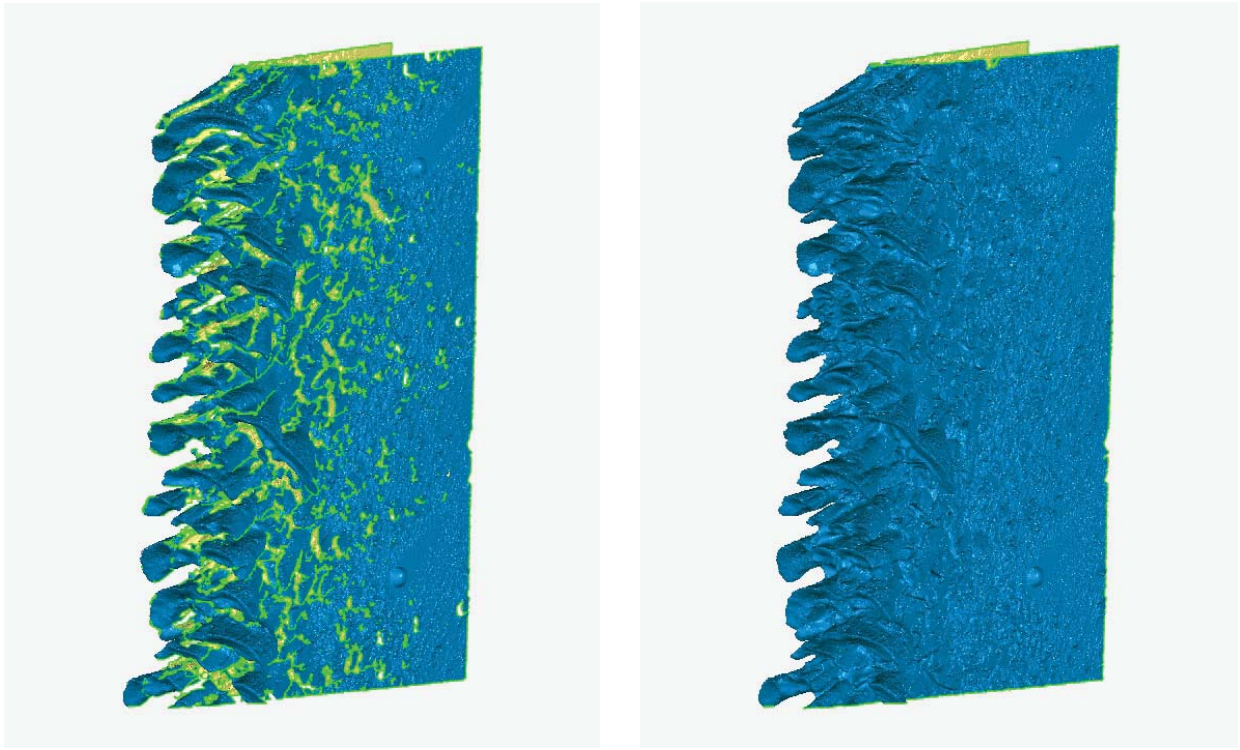

a) Mesh holes after Wrap function **b) Mesh after made water-tight.**

Figure 12 Scallop ice immediately after meshing and after processed into water tight surface.

D. Editing Mesh with Repair Tools

The holes in the mesh shown in Figs 11a and 12a were the result of un-scanned regions in the mesh surface. They could also be caused by defects in the surface mesh. Before the holes can be filled, these defects needed to be repaired using a Geomagic Studio tool called Mesh Doctor. It was used to analyze the mesh in order to find and remove the following:

Non-manifold Edges: Triangles that are on the natural boundary of the object, but not connected on two sides of the triangles sides.
Self-intersections: Triangles tangled or intertwined with neighboring triangles.
Small Components: Free-standing triangles that are so few in number they represent noise.
Small Tunnels: Double-layered constructs in the mesh with a front and back opening.

The Mesh Doctor process usually resulted in additional holes since the defective surface was removed. The holes were filled by either manually selecting individual holes or by using the Fill All function which automatically selected and filled all of the holes. There were three hole-contouring methods that Geomagic can use to fill the holes: Curvature, Tangent, and Flat. The Curvature fill starts tangent to edges and ends tangent on curve projection. However, this modifies the mesh surrounding the hole. The Tangent fill starts tangent to edges and projects a flattened curve that does not modify the mesh surrounding the hole. The Flat fill is flat and level. In this study, the Tangent fill was primarily used to fill the holes, with the Flat fill being used only to fill holes that were very difficult to fill. The Curvature fill was never used because the manner that it modified the surrounding mesh could not be controlled.

Geomagic also had three Fill modes which were utilized depending on the size and complexity of the holes. These dictated how much of the hole to fill. The Complete Fill mode filled a closed boundary and was used to fill small, simple holes, as shown in Fig. 13. The Partial Fill mode filled between two selected points and a boundary and was used to fill larger holes in segments (Fig. 14). The Bridge Fill mode connected one boundary to another and was primarily used to connect two separated surfaces, which often occurred with scallop ice shapes, as shown in Fig. 15.

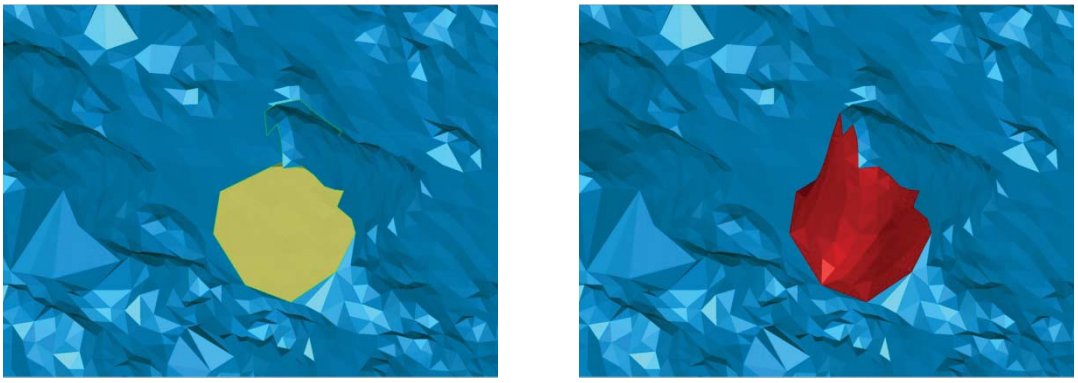

a) Before **b) After**

Figure 13 Complete Fill method.

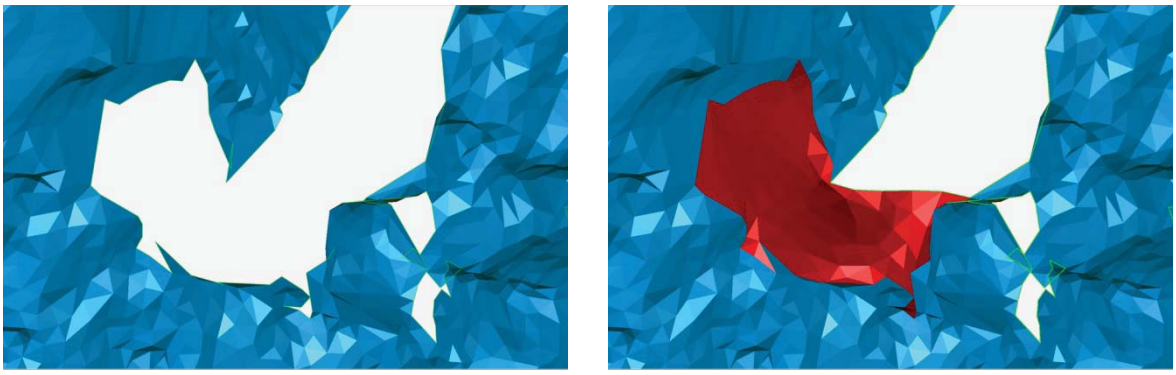

a) Before **b) After**

Figure 14 Partial Fill method.

a) Before **b) After**

Figure 15 Bridge Fill method.

Filling the holes often resulted in additional defects in the mesh usually due to problems with the hole edges that Mesh Doctor did not detect prior to being filled. Thus, the Mesh Doctor-Fill holes routine was repeated until all of the holes were filled and the mesh was water-tight.

E. Coordinate Alignment

The geometric coordinates of all of the surfaces digitized by the scanner were originally referenced to the base of the scanner. Before the data can be used, the coordinate system of the data needed to be translated to the coordinate system of the airfoil model. This was done through the use of reference hard-points that were measured with the ice shape scans.

The first step was generating the reference points for the airfoil models. This was done by utilizing the five planes from inside of the removable leading edge of the CAD model of the airfoil. The five planes generated from the hard probing of the model (shown in Fig. 6a) were aligned to the corresponding planes from the CAD model. In the process, the hard probed reference points of the counter sink holes were moved to the coordinate system of the model. These points could now be used as the airfoil reference points for all subsequent ice scans on this model.

The ice scans were transformed from the scanner-based coordinate system to the airfoil model coordinate system by aligning the five hard probe points of the reference holes taken during the scan to the model reference points. Because the hard probes points taken during the ice scans were associated with the ice scans, moving the hard probe points moved the scanned ice as well.

F. Converting Scan Data into RPM models

For the straight-wing validation of the laser scanning system, the ice scans were manufactured into wind tunnel test articles so that they could be compared aerodynamically to the traditional mold/cast versions of the same ice

accretion. In order to do this, the scans needed to be converted into leading edge RPM models with built-in pressure taps that could be attached to the leading edge of the airfoil model.

The airfoil model used for the aerodynamic testing had a span of 33.56 inches, and the ice shape leading edge was split into three spanwise segments of equal length (11.17 inches), each having identical ice shape. The first step in the process was to trim the ice shape scans into 11.17-inch spanwise segments. The exact location of the cuts were chosen to minimize the differences between the ends since one end of one ice shape needed to joined to the end of the adjoining ice shape. Using the CAD model of the clean leading edge as a guide, the scanned ice were converted into artificial ice leading-edge shapes that could be attached to the airfoil model as shown in Fig. 16. This included the mounting holes that were needed to attach the artificial ice shapes to the airfoil model.

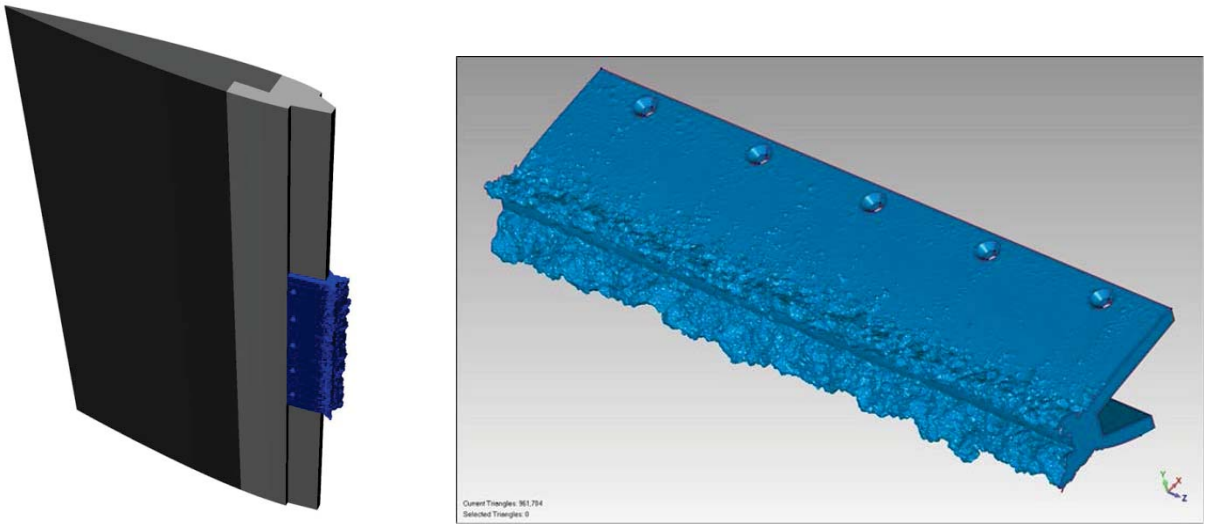

Figure 16 Artificial ice shape leading-edge model.

The final step in the process to generate the RPM model was to generate the holes for the pressure taps. This was done by first generating the plugs for the pressure taps in CAD software, as shown in Fig. 17. The diameter of the plugs was 0.05-in so that 0.04-in stainless-steel tubes could be flush mounted to the surface of the artificial ice shape. In complex areas of the ice shape, such as a glaze horn, the holes required a turn, or change in direction, so the stainless steel tubes could not be flush mounted to the surface.

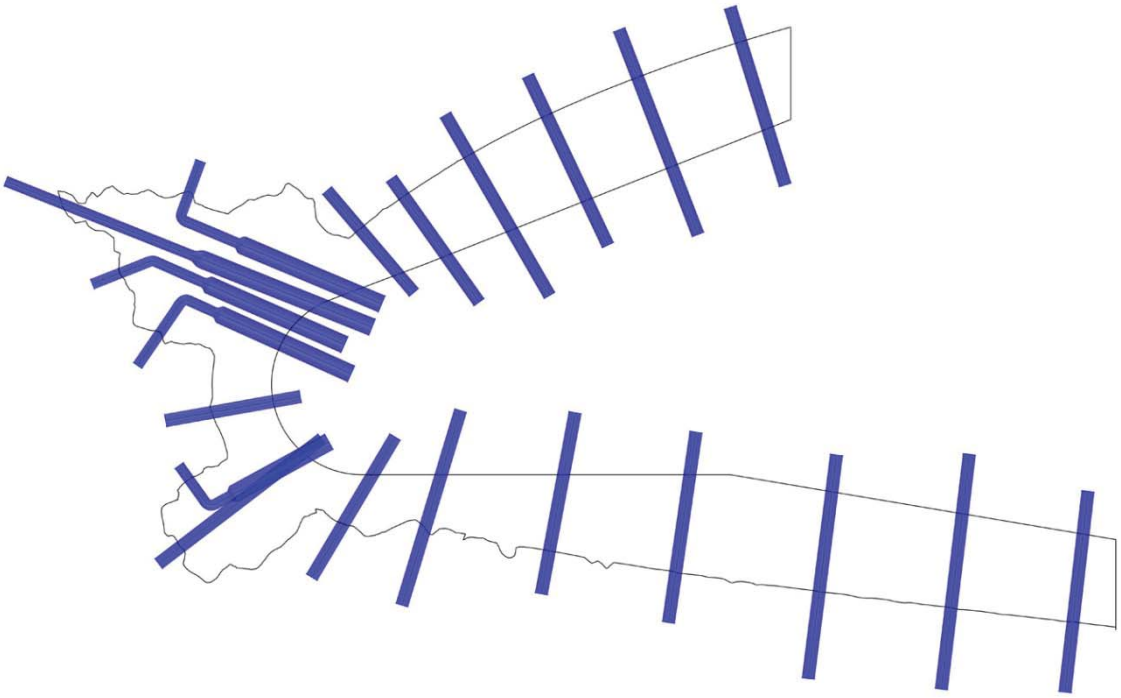

Figure 17 Pressure tap plugs generated using CAD.

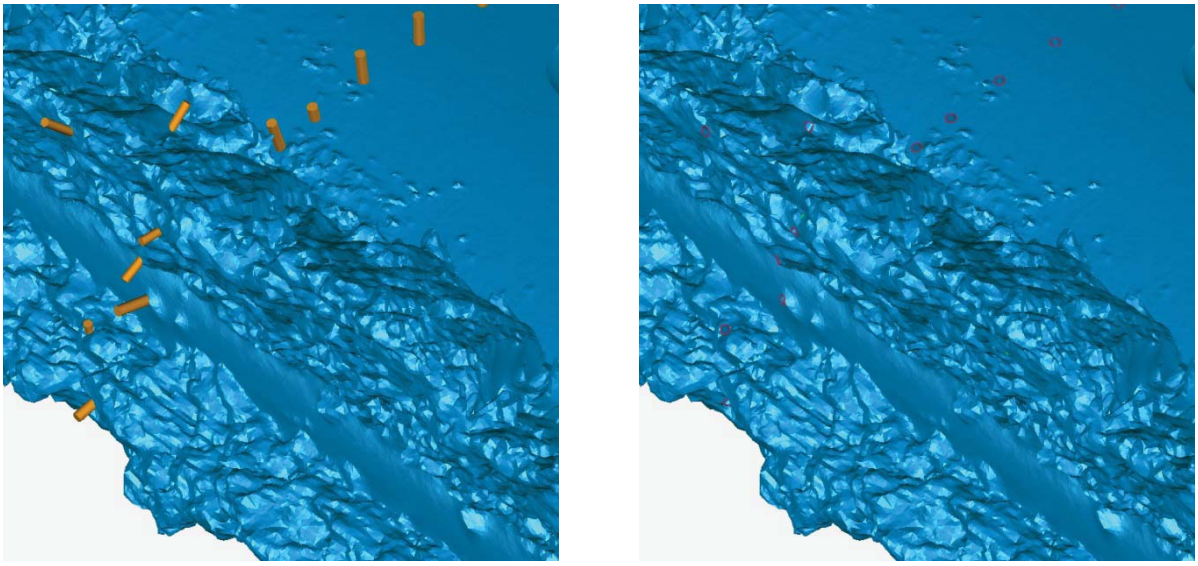

a) Before Boolean subtract **b) After Boolean subtract**

Figure 18 Boolean subtract operation to cut pressure tap holes on the ice shape model.

These pressure tube plugs were then Boolean subtracted from the ice shape CAD model resulting in the pressure tap holes shown in Fig. 18. Figure 19 shows the close-up photo of the pressure taps on the RPM ice shape.

Figure 19 Pressure taps on artificial RPM ice shape.

IV. Benchmark Measurements

The first step in the Phase II implementation and validation portion of the 3-D scanner development was performing benchmark measurements on a known "roughness benchmark" block, as shown in Fig. 20a. It was used to provide a simulation of ice roughness on a glaze ice accretion. It was constructed of aluminum and consisted of hemispheres of known size and pattern. Four patterns were scanned for the benchmark study: 0.063-in diameter standard spacing, 0.063in-diameter tight spacing, 0.047in diameter standard spacing, and 0.031-in diameter tight spacing. On the standard spacing, the hemispheres were placed 2 diameters apart from the center. On the tight spacing, the hemispheres were arranged with hexagonal tight packing, with the beads touching one another at the base.

Figures 20b-e show the comparison between the idealized geometry of the roughness block and the scan of the roughness block. The deviation scales shown on the right side of the figures are in inches and the reference is the scan data and the test surface is the idealized geometry. The results show that scanner was able to capture hemispherical beads as little as 0.031in diameter. The tops of the hemispheres were usually within 0.003in of the idealized geometry for all of the cases except the 0.063in-diameter tight spacing, which were up to 0.008in taller. This was due to the manufacturing errors in the calibration block and not due to scan errors (and was verified with caliper measurements).

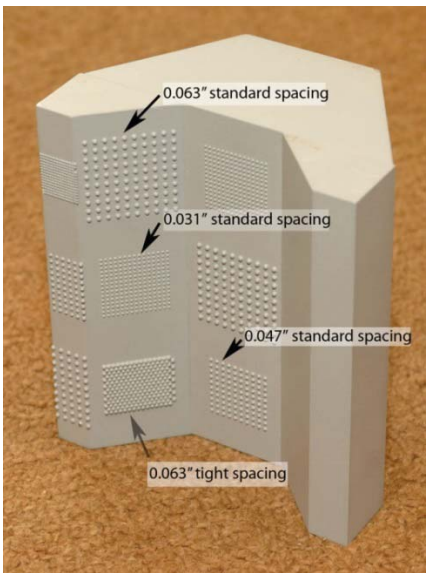

a) Roughness benchmark block

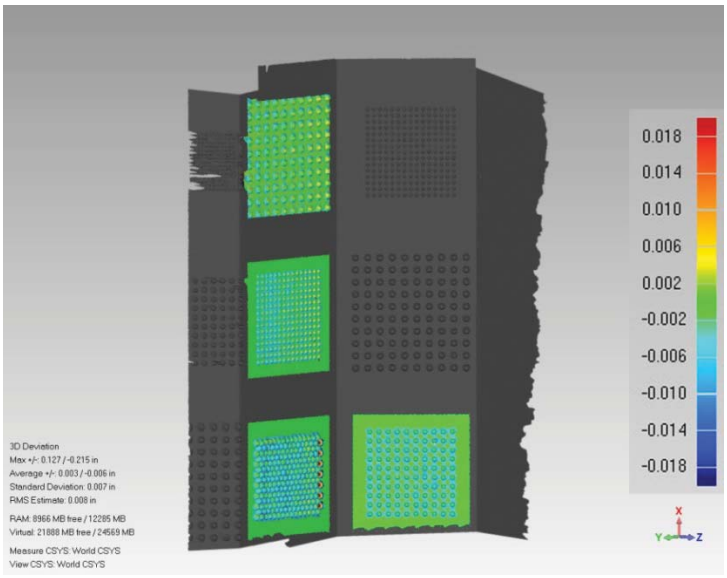

b) Benchmark block deviation

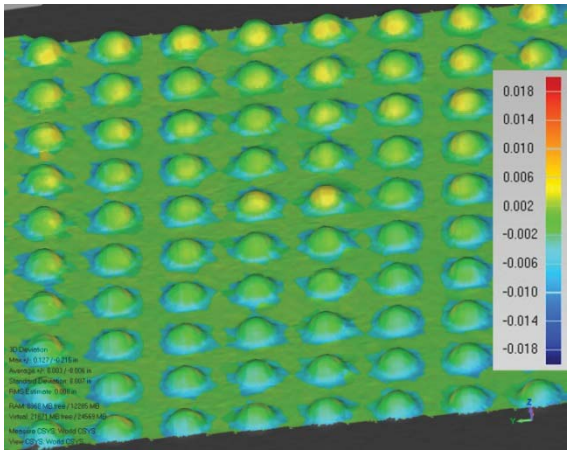

c) 0.063" standard spacing deviation

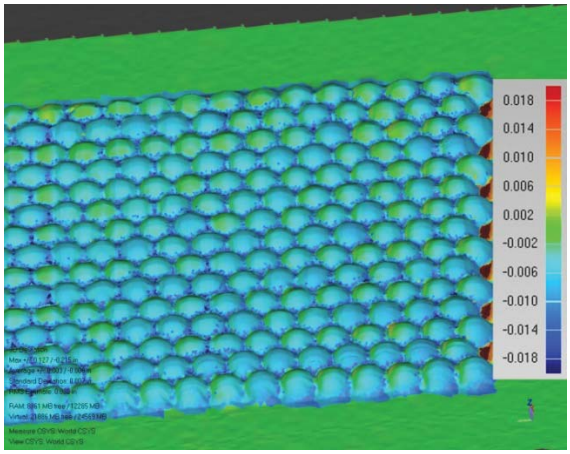

d) 0.063" tight spacing deviation

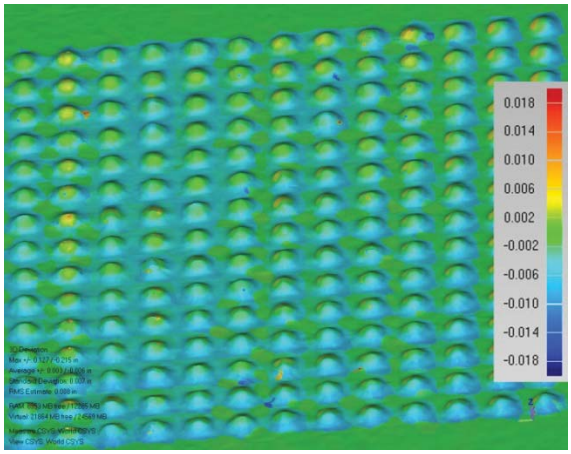

d) 0.031" standard spacing deviation

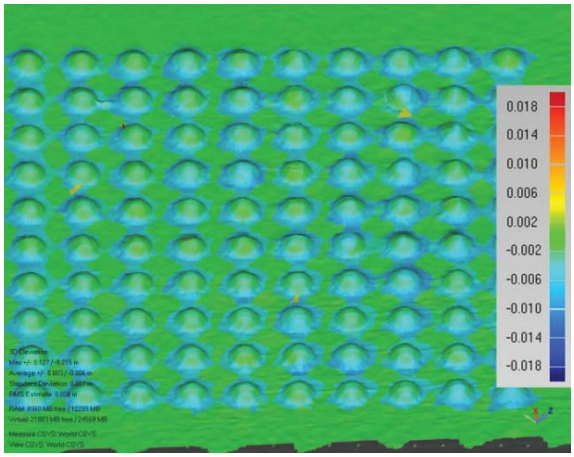

e) 0.047" standard spacing deviation

Figure 20 Roughness benchmark block evaluation.

V. 2-D Airfoil Validation

As stated in the introduction, the main component of the Phase II validation and implementation effort was the "circular" geometric and aerodynamic assessment on a 2-D (straight wing) airfoil geometry. For this study a glaze (horn) ice accretion, two ice roughness ice accretions, two rime (streamwise) ice accretions, and a runback (spanwise-ridge) ice accretion were chosen. The icing conditions used to generate the shapes are shown in Table 1.

Table 1 Ice shapes tested for straight wing.

Ice Shape	Run Number	α (°)	V (kts)	LWC (g/m^3)	MVD (μm)	T_0 (°C)	Spray (min)
Glaze (Horn)	ED1978	2	200	0.75	15	-2.2	5
Roughness	ED1974	2	200	0.75	15	-2.2	0.5
Roughness	ED1983	2	200	0.4	30	-17.8	1
Rime (Streamwise)	ED1977	2	200	0.4	30	-17.8	5
Rime (Streamwise)	ED1966	5	175	0.3	15	-17.8	5
Runback (Spanwise Ridge)	ED1967	1	175	0.64	15	-4.4	9.5

The scan data of the ice accretions were processed into water-tight surfaces using Geomagic, as described in the previous section. They were then turned into removable leading-edge artificial ice shapes for testing on an 18-in chord NACA 20312 airfoil model in the University of Illinois aerodynamic wind tunnel. They were constructed using both stereo lithography and High Density PolyJet rapid prototype manufacturing methods. An initial assessment performed by Lee, et al[6] showed that for most ice shapes, the SLA method was sufficient to produce all of the relevant ice features required for the aerodynamic assessment. However, for one of the roughness cases (ED1983), both SLA and PolyJet HD were used to compare the results. The properties of the two methods are shown in Table 2.

Table 2. Properties of rapid prototype methods

Process	Min. Layer Thickness (in)	Tolerance (in)	Min. Feature (in)
SLA	0.005	+/- 0.015	0.025
HD PolyJet	0.0006	+/- 0.005	0.012

Three identical 11.17" spanwise segments of the ice shapes were required to span the leading edge of the aerodynamic model. The center segments were instrumented with pressure taps. Artificial ice shapes were also constructed using the traditional mold/casting methods for both geometric and aerodynamic comparisons. The results of the aerodynamic comparison between the RPM shapes and the cast shapes are included in a companion paper by Broeren et al.[12] This paper presents the results and analysis of the geometric comparison between the RPM shapes and the cast shapes.

Both the RPM and the cast ice shapes were mounted on the leading edge of the aerodynamic model and scanned with the Romer laser scanner. The casting and PolyJet ice shapes were slightly translucent, and they required a light surface coating with white spray primer. The SLA shapes did not require any surface treatment in order to be scanned as it was infused with a grey pigment, making them sufficiently reflective.

A. Run ED1978-Glaze (Horn) Ice Accretion

Figure 21 shows the results from the run ED1978, which was a glaze ice accretion. Figure 21a shows the CAD model of the RPM ice shape that was tested in the aerodynamic wind tunnel. Figure 21b shows the 2-D cross sectional cuts of the scanned ice accretion, SLA shape, and the cast shape at the location of the pressure tap row. Figure 21c shows the 3-D deviation of the scan of the manufactured SLA shape from the CAD model from which it was manufactured. The CAD model is essentially the scan of the original ice accretion. The plot on the left shows the upper (suction) surface and the plot on the right shows the lower (pressure) surface. The scale of the plot is in inches where positive values are when the scan of the SLA is larger when compared to the ice shape scan. Figure 21d shows the 3-D deviation of the scan of the cast ice shape from the scan of the original ice accretion.

Figure 21 shows that the scan of the SLA shape compared very well with the scan of the ice accretion. Large areas of the scans (especially the ice horn areas) were within 0.01-in. Nearly all of the ice shape was within 0.02 in.

The regions of high deviation on the side of the ice shape and the mounting holes were due to the fact that these regions were not scanned for the SLA shape. These results showed that the SLA ice shape was manufactured and mounted on the leading edge of the aerodynamic model with a high degree of accuracy.

There were larger differences between the scan of the casting and the ice accretion scan, as Figure 21b and 21d show. Figure 21b shows that the upper surface horn on the casting was 0.10-in shorter than the horn on the original ice accretion. There also appeared to be a part of the ice shape missing on the base of the upper surface horn in the casting. This is also shown by the 3-D deviation plot of Fig. 21d. The upper surface horn of the casting was generally smaller than the original ice accretion, most likely due to mold/casting shrinkage and warping. There were also many gray regions shown on the plot, which was indicative of missing features on the scan of the casting. These were likely fragile features such as feathers that were lost during the mold/casting process. These differences resulted in an aerodynamic difference between the SLA and cast shape, with the cast ice shape having a maximum lift coefficient that was 5% higher than the SLA shape.[12]

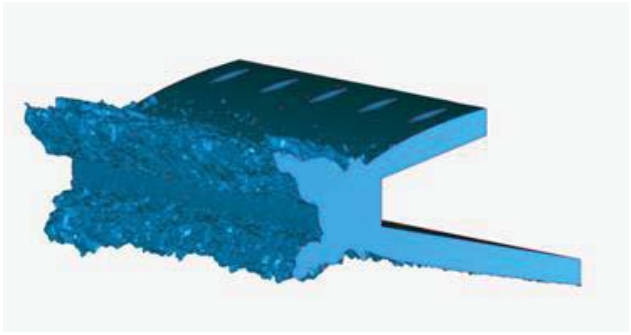

a) Leading-edge model

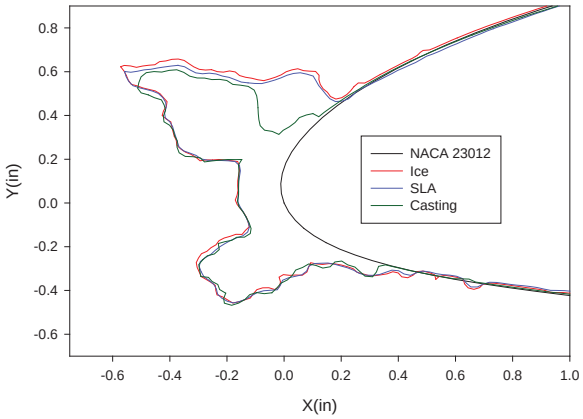

b) Cross section cuts

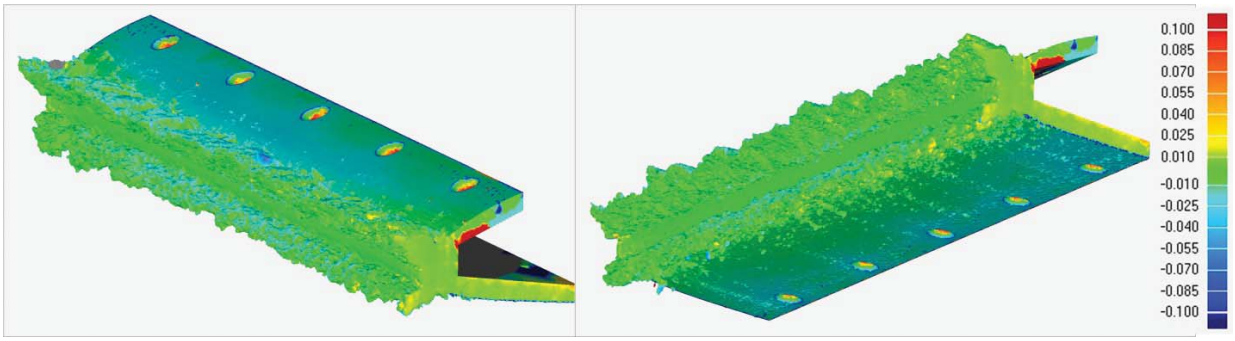

c) SLA deviation plots (left: upper surface and right: lower surface)

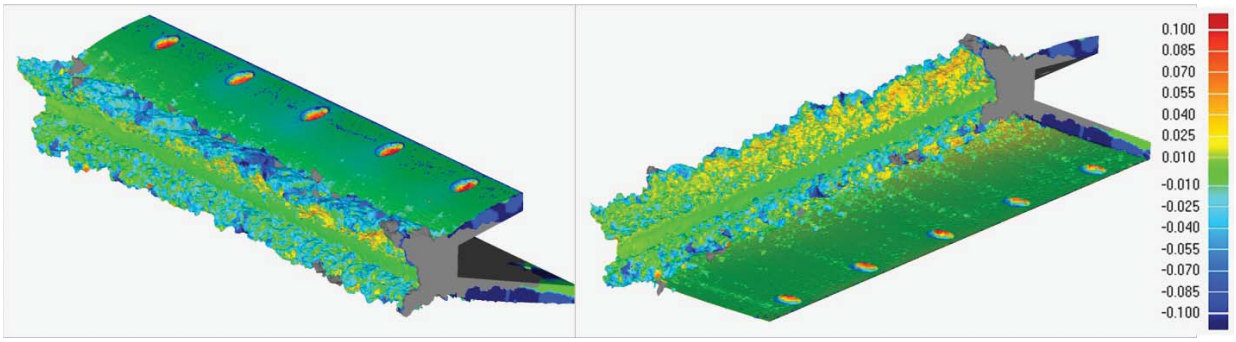

d) Casting deviation plots (left: upper surface and right: lower surface)

Figure 21 Horn ice RPM/casting comparison (ED1978).

B. Run ED1974 – Roughness Ice Accretion

Figure 22 shows the comparison plots for the roughness ice accretion from run ED1974. The plots of the cross section cuts are shown in Fig. 22b and show that both the SLA and casting shapes agree well with the original ice accretion scan. The cross section of the cast scan is inside the airfoil surface at some areas. This was attributed to possible shrinkage in the mold/casting process, similar to that observed for run ED1978, but not as significant. The 3-D deviation plots shown in Figs. 22c and 22d also show that both the SLA and cast shapes agree well with the original ice accretion scan. The SLA scan was mostly within 0.01-in of the original ice scan, and the casting scan was generally within 0.02in of the original ice accretion scan.

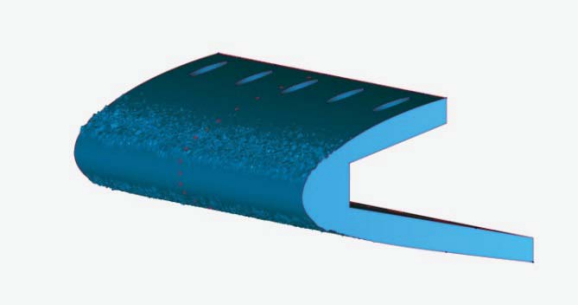

a) Leading-edge model

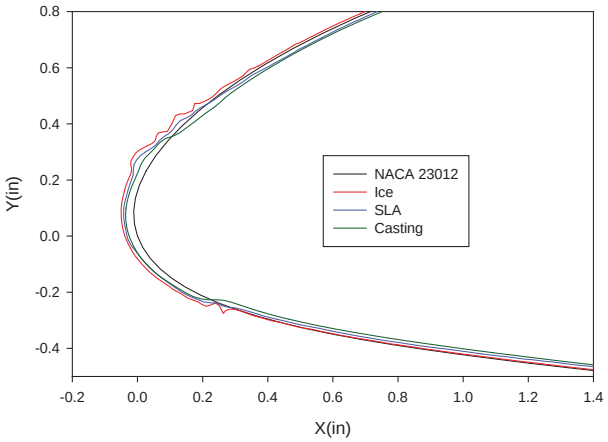

b) Cross section cuts

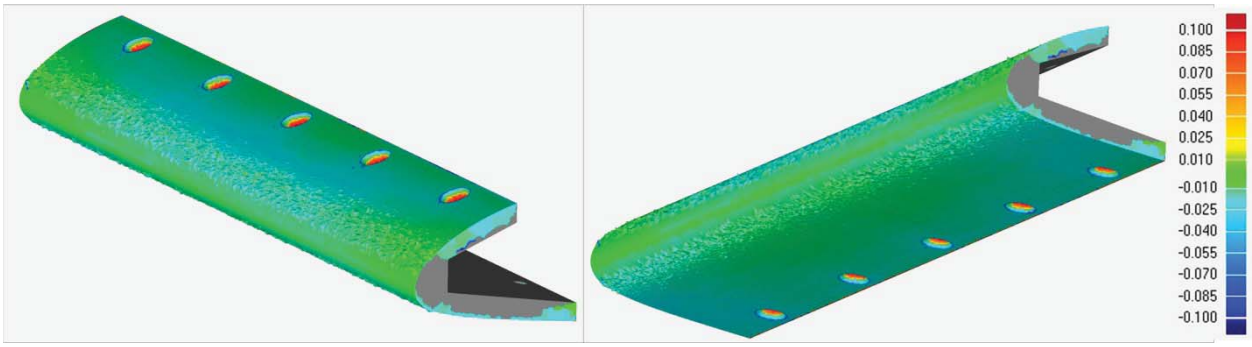

c) SLA deviation plots (left: upper surface and right: lower surface)

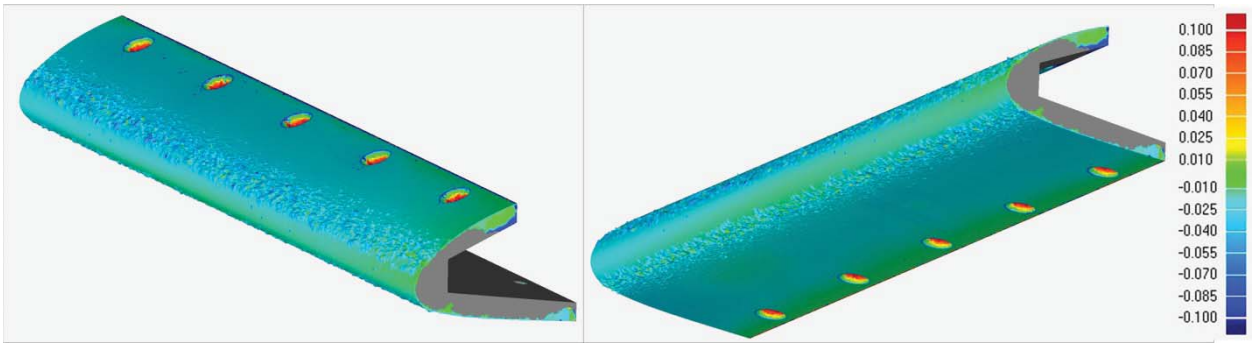

d) Casting deviation plots (left: upper surface and right: lower surface)

Figure 22 Roughness RPM/casting comparison (ED1974).

Figure 23 shows the close-up comparison of the roughness features on the ice shape. A section of the ice shape on the upper surface was isolated for both the SLA and the casting shape, since the local roughness features are aerodynamically more important than the overall ice shape. They were aligned to the corresponding region in the original ice scan using a best-fit alignment in order to compare just the local roughness features and not the overall ice shape. Figure 23a shows that SLA was mostly within 0.005-in of the ice accretion scan. The roughness from the casting did not fit as well, with some regions that were up to 0.02-in shorter than the ice accretion scan while some regions were 0.02-inch taller than the ice accretion scan. Given that the typical roughness height of this shape was 0.02-in, this may have been due to the ice accretion scan missing some roughness features and the casting having lost some roughness feature in the mold/casting process.

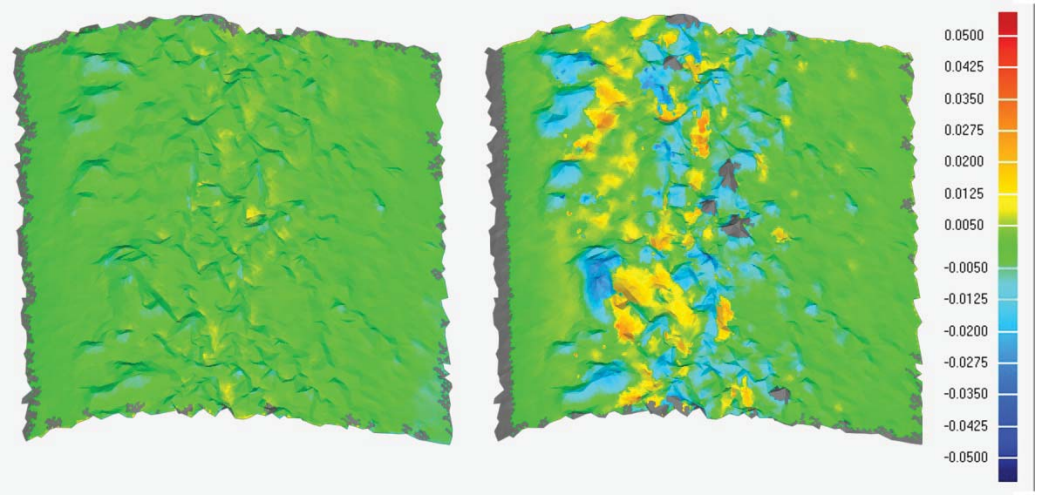

a) SLA **b) Casting**

Figure 23 Roughness deviation map - ED1974

C. Run ED1983 - Roughness Ice Accretion

Figure 24 shows the comparison plots for the second roughness ice accretion from run ED1983. This icing condition resulted in much smaller roughness, with a typical roughness height of 0.002-in. For this condition, an RPM artificial ice shape was constructed of PolyJet HD as well as SLA in order to determine any differences between these two methods. The plots of the cross section cuts are shown in Fig. 22b and show that both the SLA and PolyJet shapes agreed well with the original ice accretion scan. The cast shape was undersized, similar to what was observed for the horn shape. The 3-D deviation plots shown in Figs. 22c to 22e also show that both the SLA and PolyJet shapes agree well with the original ice accretion scan. The SLA shape was mostly within 0.02-in, while the PolyJet shape was mostly within 0.01-in. The ice casting scan was undersized by as much as 0.07-in on the upper surface.

Figure 25 shows the close-up comparison of the roughness features over a small section of the ice shape. Again, the scans of the SLA, PolyJet, and casting were aligned to the corresponding region in the ice accretion scan using a best-fit alignment in order to compare just the local roughness feature and not the overall ice shape. Figures 25a and 25b show that SLA and PolyJet shapes were mostly within 0.005-in of the ice accretion scan. The roughness from the casting did not fit as well, with some regions that were up to 0.01-in shorter than the ice accretion scan while some regions were 0.01-in taller than the ice accretion scan. This roughness size (0.002-in) was likely beyond the ability of the scanner to measure the ice and the RPM method to reproduce the ice shape. Table 2 shows that this roughness height is well below the minimum layer height of the SLA manufacturing method. Although the PolyJet method was capable of manufacturing layers of this height, its tolerance was greater than the roughness height. This was verified by the aerodynamic results shown in Broeren et al.[12] that showed that the maximum lift coefficients of the SLA and PolyJet ice shapes were 6% and 11% higher than the cast shape.

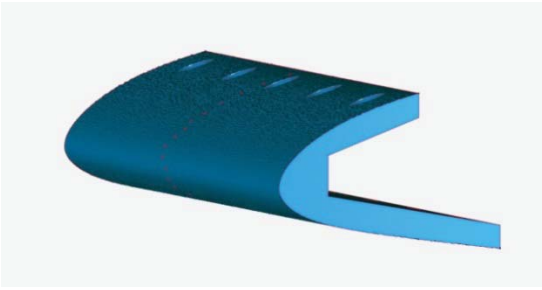

a) Leading-edge model

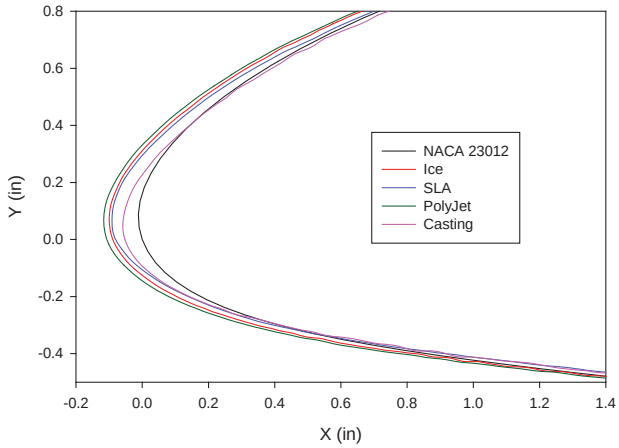

b) Cross section cuts

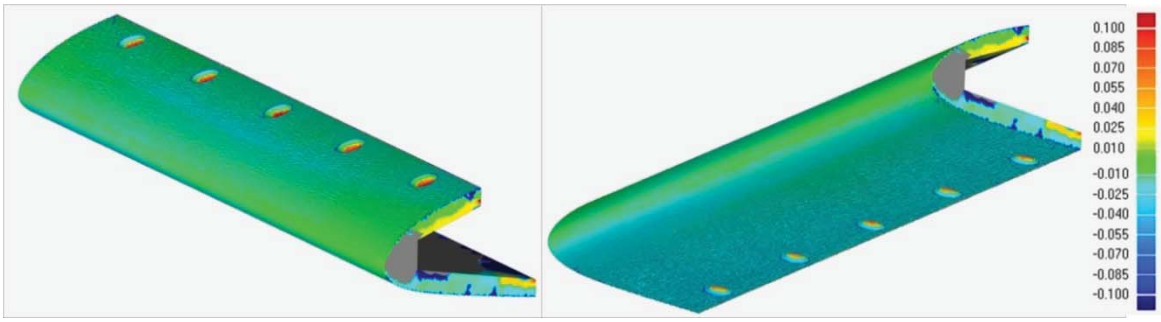

c) SLA deviation plots (left: upper surface and right: lower surface)

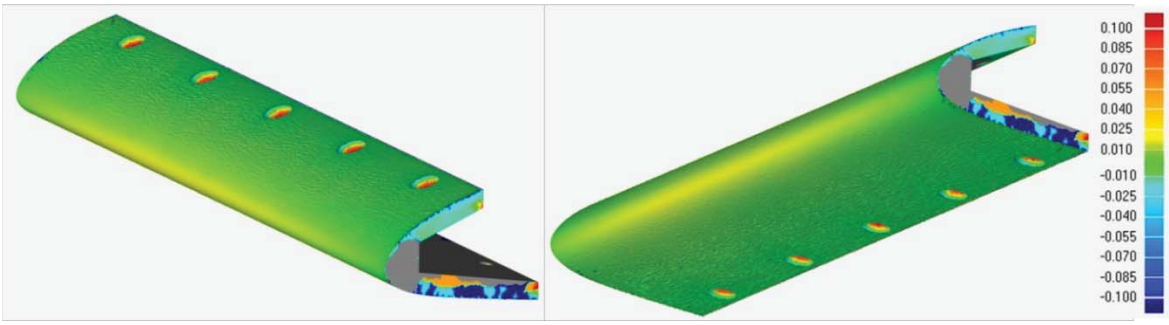

c) PolyJet HD deviation plots (left: upper surface and right: lower surface)

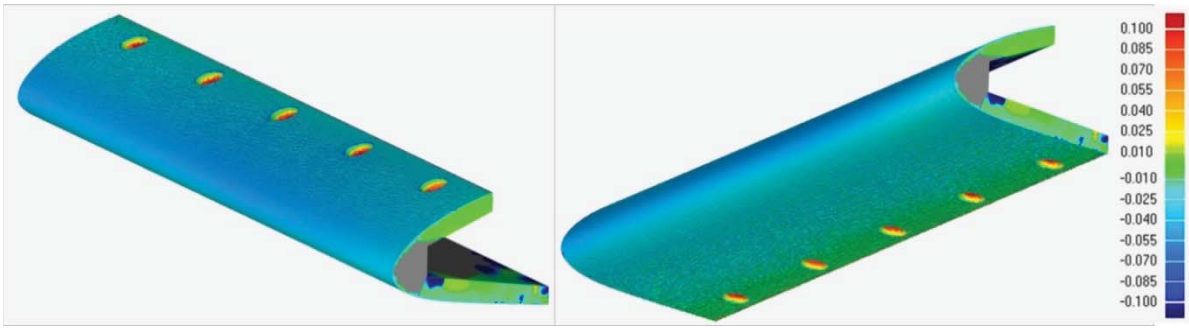

d) Casting deviation plots (left: upper surface and right: lower surface)

Figure 24 Roughness RPM/casting comparison (ED1983)

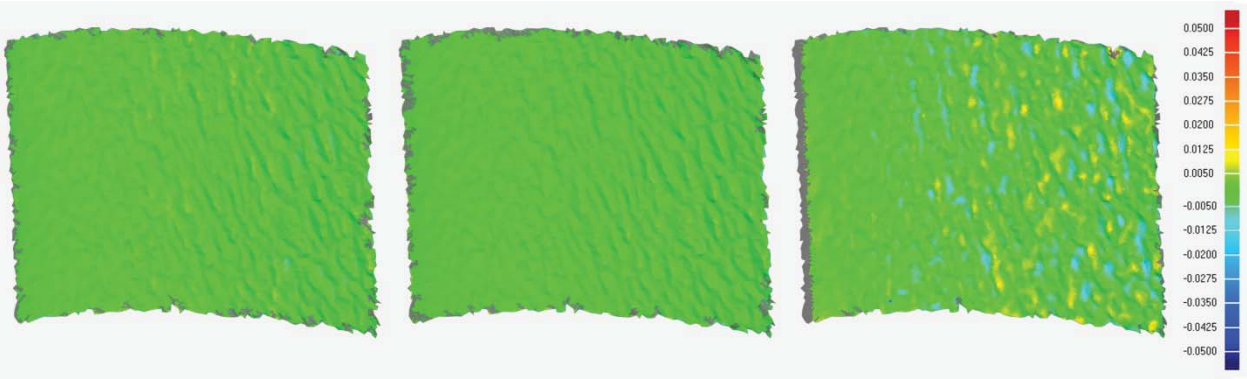

a) SLA **b) PolyJet HD** **c) Casting**

Figure 25 Local roughness deviation map - ED1983

D. Run ED1977-Rime-Streamwise Ice Accretion

Figure 26 shows the comparison plots for the rime ice accretion from run ED1977. The plots of the cross section cuts are shown in Fig. 22b and show that the SLA shape agreed very well with the original ice accretion scan while the cast shape was slightly undersized. The 3-D deviation plots shown in Figs. 26c and 26d show that the SLA shape deviated less than 0.01-in in the smooth stagnation zone. There was larger amount of deviation in the roughness feather zones. Some of this was probably due to slight spanwise misalignment between the SLA scan and the original ice accretion scan. The casting scan was undersized by 0.02-inch in the smooth zone and by up to 0.07-inch in the rough, feather regions. Again, some of this may have been due to a combination of misalignment of the scans and general shrinkage in the casting process.

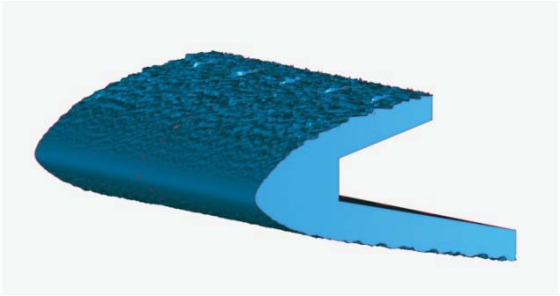

a) Leading-edge model

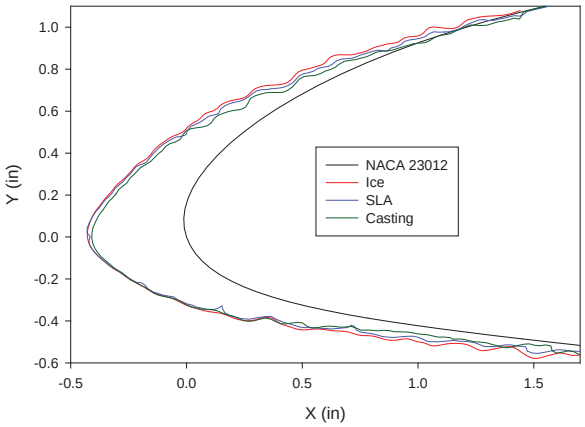

b) Cross section cuts

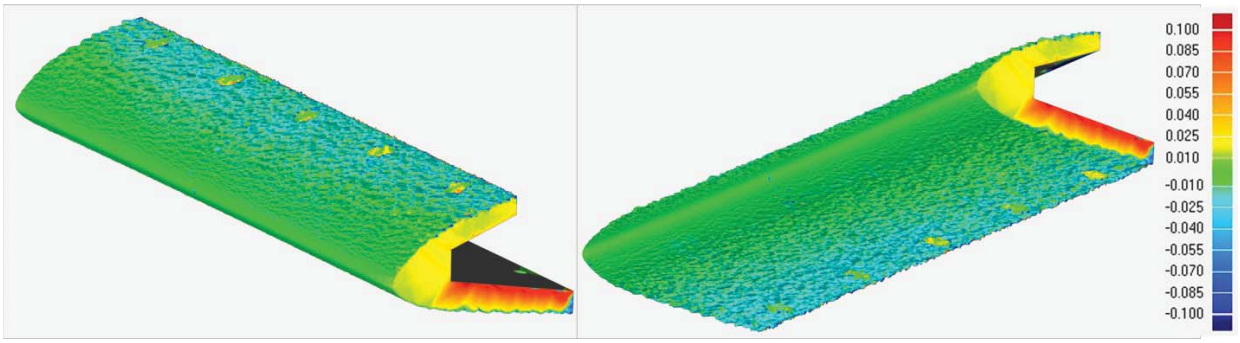

c) SLA deviation plots (left: upper surface and right: lower surface)

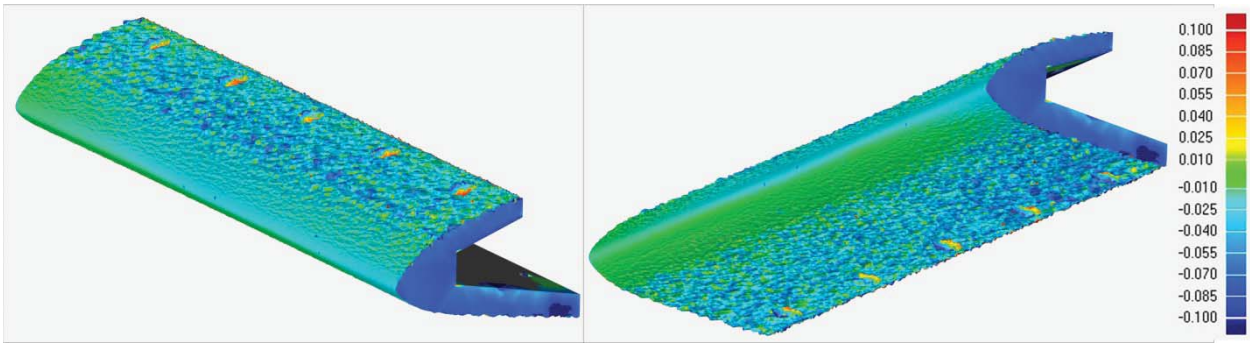

d) Casting deviation plots (left: upper surface and right: lower surface)

Figure 26 Streamwise RPM/casting comparison (ED1977).

Figure 27 shows the close-up comparison of the roughness features over a small section of the rime ice shape. Figure 27a shows that the SLA shape was mostly within 0.005-in of the ice accretion scan when the surfaces were properly aligned. The roughness from the casting did not fit as well, with some regions that were up to 0.02-in shorter than the ice accretion scan while some regions were 0.02-in taller than the ice-accretion scan. There were also some roughness features that were missing from the casting, as shown by regions that are gray. However, the two ice shapes were aerodynamically equivalent, with nearly identical lift curves and drag polars.[12]

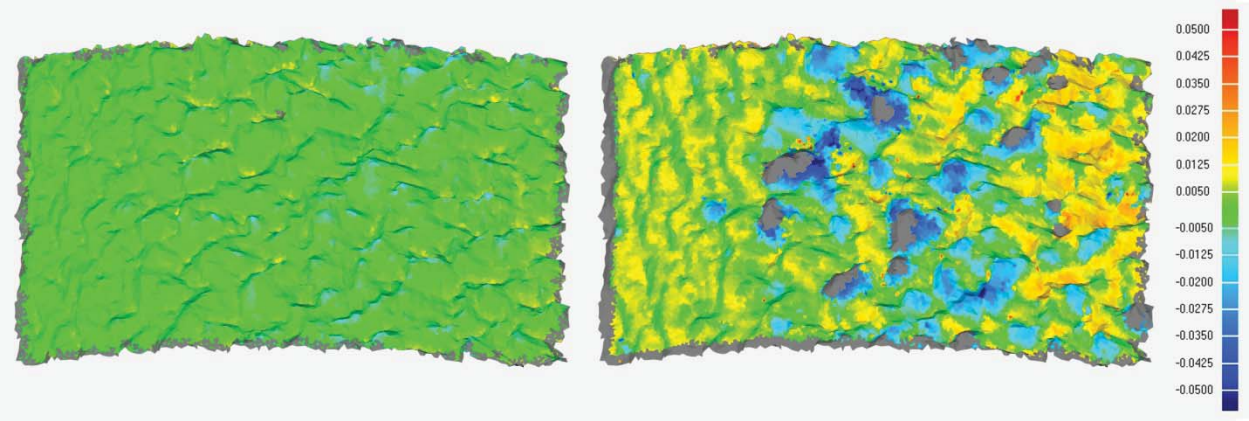

a) SLA **b) Casting**

Figure 27 Local roughness deviation map - ED1977

E. Run ED1966-Rime-Streamwise Ice Accretion

Figure 28 shows the comparison plots for the second rime ice accretion from run ED1966. The plots of the cross section cuts are shown in Fig. 28b and show that the SLA shape agreed very well with the original ice accretion scan, while the cast shape was slightly undersized. The 3-D deviation plots shown in Fig. 28c show that the SLA shape deviated less than 0.01-inc for a large area of the ice shape. The casting scan was undersized by as much as 0.07-in in the rough feather zone on the upper surface. Some of this may have been due general shrinkage in the casting process.

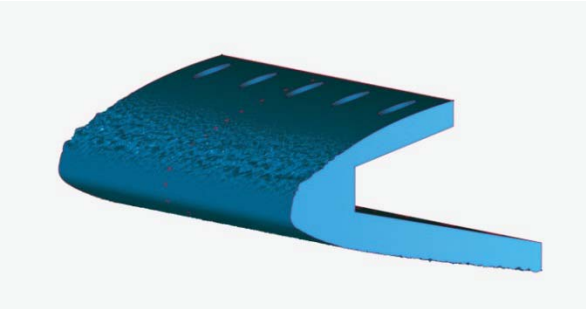

a) Leading-edge model

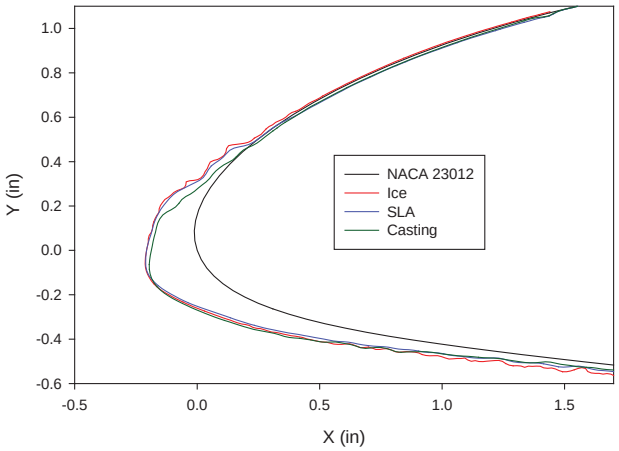

b) Cross section cuts

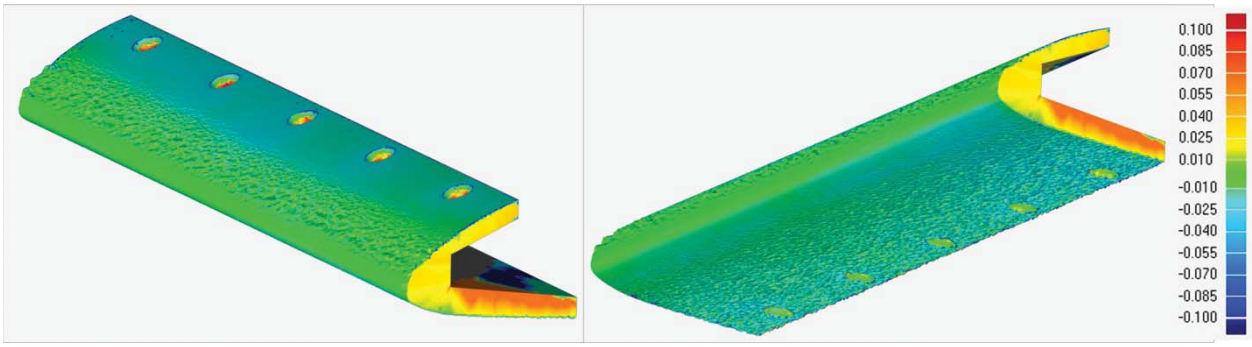

c) SLA deviation plots (left: upper surface and right: lower surface)

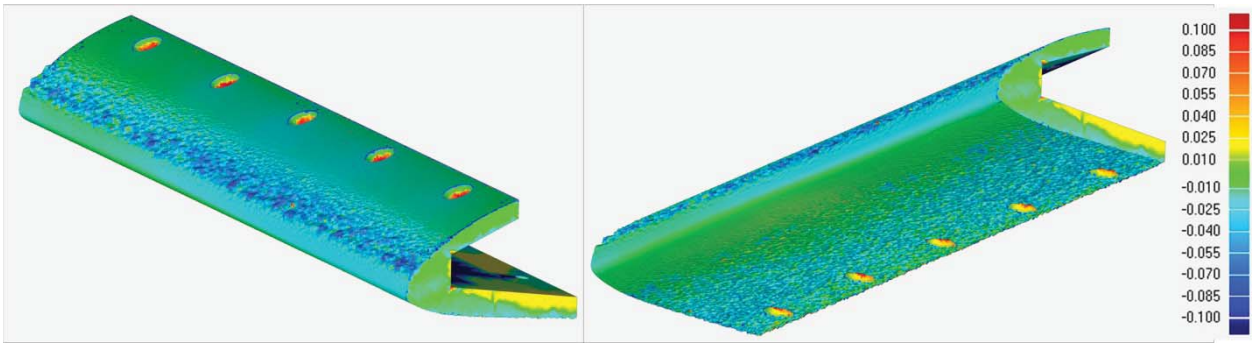

d) Casting deviation plots (left: upper surface and right: lower surface)

Figure 28 Streamwise RPM/casting comparison (ED1966).

Figure 29 shows the close-up comparison of the roughness features over a small section of the ice shape. Figure 29a shows that the SLA shape was mostly within 0.005-in of the ice accretion scan when the surfaces were properly aligned. The roughness from the casting did not fit as well, with some regions that were up to 0.02-in shorter than the ice shape scan while some regions were 0.02-in taller than the ice-accretion scan. There were also some roughness features that were missing from the casting, as shown by regions that are gray. Because of these missing features, there was probably some significant error in the automated best-fit alignment between the casting and the ice scan, even more than what was observed for ED1977 (Fig.27). This made the comparison of the local features on the cast shape to those on the original ice scan less meaningful. However, the SLA and cast shapes were

aerodynamically nearly identical, with the maximum lift coefficient within 0.1% and drag in the linear portion of the lift curve within 3%.[12]

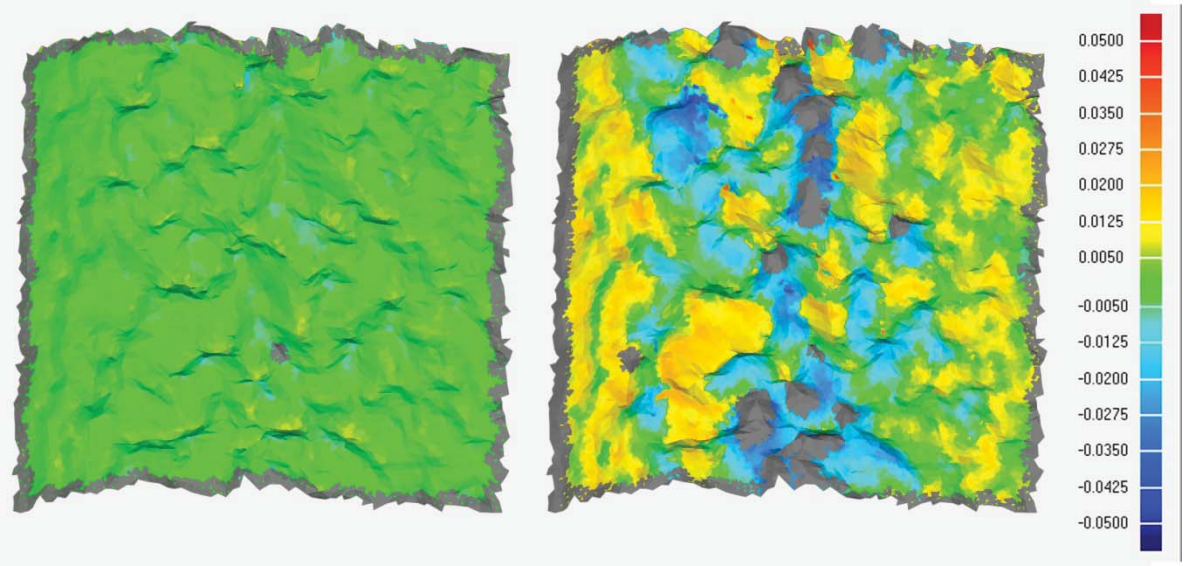

a) SLA **b) Casting**

Figure 29 Local roughness deviation map - ED1966

F. Run ED1967-Runback-Spanwise Ridge Ice Accretion

Figure 30 shows the comparison plots for the runback ice accretion from run ED1967. In order to produce the runback shape, an electro-thermal heater was adhered to the leading edge of the model to prevent the impinging water from freezing. The water flowed downstream and froze on an unheated portion of the model forming a runback ridge on the upper and lower surfaces. The electro-thermal heater surface could not be scanned along with the runback ice accretion because it was too reflective. It could also not be painted because it would have been too difficult and time consuming to remove the paint prior to the next test run. Because of this, the heater was simply taped over prior to painting the ice. In order to create the CAD model for the manufacture of the RPM shape, the clean NACA 23012 airfoil section was blended into the scan of the runback ice shape. For the cast shape, a mold was made with the heater still attached to the leading edge, so the casting included the heater which added approximately 0.03 in to the leading edge thickness.

The plots of the cross section cuts are shown in Fig. 30b and show that the SLA shape agreed very well with the original ice accretion scan while the cast shape was undersized. The 3-D deviation plots shown in Fig. 30c show that the SLA shape deviated less than 0.02-inch for most of the ice shape. There was a large amount of deviation at the downstream edge of the ice accretion where there are missing features on the SLA shape. This was the ice that formed on the seam of the removable leading edge that was scanned but removed prior to casting. It was also removed on the SLA after it was built (in order to be consistent with the cast shape), but it was still present in the original ice accretion scan. Figure 30d shows that the casting scan was undersized by as much as 0.05-inch in the heater portion of the leading edge on the lower surface. This was not expected since the leading edge should have been 0.03-inch thicker than the ice scan because of the heater. However, the ice features on the casting compared very well to the ice scan, with ridge heights that were nearly identical.

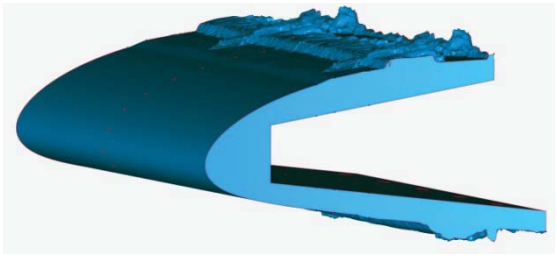

a) Leading-edge model

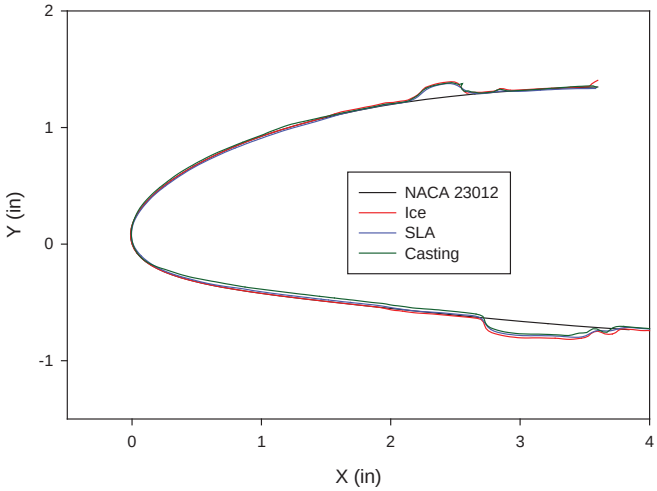

b) Cross section cuts

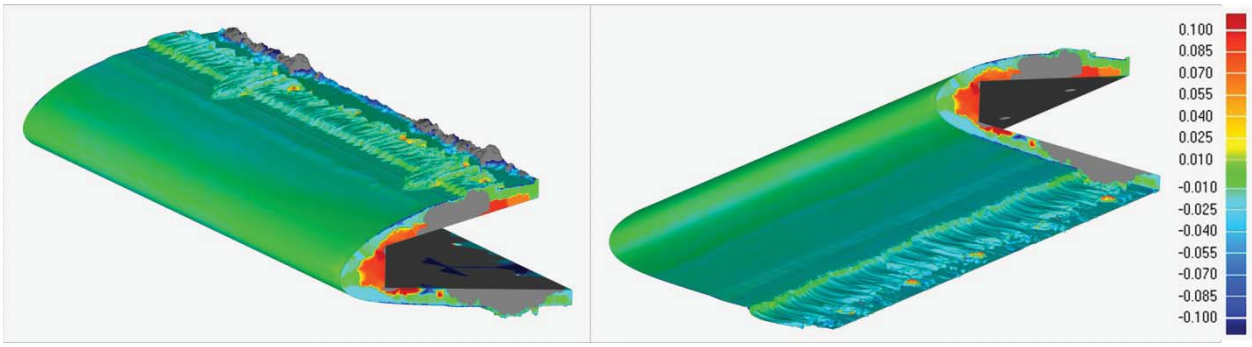

c) SLA deviation plots (left: upper surface and right: lower surface)

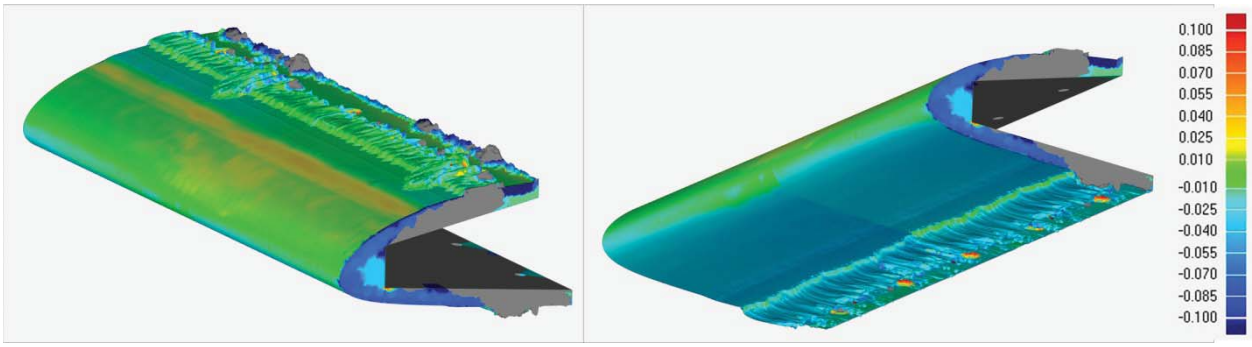

d) Casting deviation plots (left: upper surface and right: lower surface)

Figure 30 Runback ice RPM/casting comparison (ED1967).

G. 2-D Wing Ice Comparison Summary

The results from geometric comparisons on the straight wing showed that the ice shape models generated through the scan/RPM process compared very well with the original ice accretion scans. The RPM manufacturing process was shown to reproduce the original ice accretion scan normally within 0.01-inch. There were larger discrepancies between the cast ice shapes and the original ice scans. It was difficult to precisely compare the scans of the cast shapes to the original ice accretion scans because the cast shapes appear to have shrunk during the mold/casting process by as much as 0.10-inch for the glaze-horn cast shape. However, the comparisons of the local

ice shape features were possible and produced better results than the overall ice geometries. A detailed discussion of implication of these geometric differences on ice-airfoil aerodynamics can be found in Broeren et al.[12]

VI. Swept Wing Validation

The third component of the Phase II validation and implementation effort was the geometric assessment on a swept-wing airfoil geometry. Four shapes were chosen: complete scallop, incomplete scallop, roughness, and rime. Scallop ice shapes are unique to swept wings. They are very difficult to scan using line-of-sight methods, such as laser scanning, due to their complex geometry with deep, narrow gaps between scallops. Incomplete scallops are ice shapes where the scallops are not fully separated.[14] The icing conditions used to generate the shapes are shown in Table 3.

Table 3 Ice shapes tested for swept wing

Ice Shape	Run Number	Λ (°)	α (°)	V (kts)	LWC (g/m^3)	MVD (μm)	T_0 (°C)	Spray (min)
Complete Scallop	AF2037	45	0	200	0.54	32.6	-6.7	19
Incomplete Scallop	AF2032	30	4	200	0.6	15	-6.7	15
Roughness	AF2029	30	4	200	0.45	32	-7.2	3
Rime	AF2028	30	4	200	0.6	15	-17.8	15

The airfoil model used for this study was a semi-span, 36-in chord NACA 0012 model with a removable leading edge (Fig. 3b). It was mounted vertically in the test section on a turntable and could be swept at 30 and 45 deg. The scan data of the ice accretion were processed into water-tight surfaces using Geomagic. The castings of the ice shapes were made with the molds obtained during the IRT test. The castings were then scanned with the 3-D laser scanner and compared with the original scans of the actual ice. For the scallop ice shape, the casting was also digitized using a commercial computed tomography (CT) scanning service. The CT method allowed the deep gap regions between the scallops to be digitized and compared with the laser scan method, which was limited in its ability to acquire data between the scallop shapes.

Unlike on the straight wing, the cast shapes from the swept wing were not made to mount to a leading edge of an airfoil model with known reference locations. Because of this, four semi-circular rubber dots were attached to the airfoil model to provide common alignment points, as shown in Fig. 8. These dots were used to align the casting scan to the original ice accretion scans using a best fit method. However, this did not result in a very accurate fit (due to differences between the cast ice shapes and the original ice scans), so a final manual fit adjustment was required.

A. Run AF2037-Complete Scallop Ice Accretion

Figure 31 shows the results from the run AF2037, which was a complete scallop ice accretion. Figure 31a shows the fully processed scan of the ice accretion that has been made completely watertight. The top of the shape corresponds to the wing tip of the NACA 0012 model and the bottom oriented toward the model root. Figure 31b shows the 2-D cross sectional cuts of the scanned ice accretion, laser-scanned cast ice shape, and the CT scan of the cast ice shape at the centerline of the tunnel. The laser and CT scans of the casting compared very well with each other but not as well as with the scan of the original ice accretion. As with the straight wing results, the casting was smaller when compared to the original ice accretion scan, indicating that it may have shrunk or warped during the mold/casting process. This also made precise alignment of the casting scan to the original ice scan difficult. This explains the regions of casting scan that were inside the airfoil.

Figure 31c shows the 3-D deviation of the laser scan of the cast shape when compared to the original ice scan. The plot on the left shows the upper (suction) surface and the plot on the right shows the lower (pressure) surface. Figure 31d shows the 3-D deviation of the laser scan of the cast ice shape when compared to the CT scan of the same casting.

Figure 31c shows that the main scallop features of the casting deviated as much as 0.05-inch from the original ice accretion scan. There were numerous gray areas in the deviation map due to scallops and feathers that were present in the original ice accretion scan but not in the casting. These were features that broke off during the casting process. Figure 31d shows that the laser scan of the casting compared very well with the CT scan (of the same

casting), with most of the scan falling within 0.02-inch of one another. The only areas of large deviation were in the gaps between the scallops where the laser-scanner could not acquire data.

a) Water-tight scan

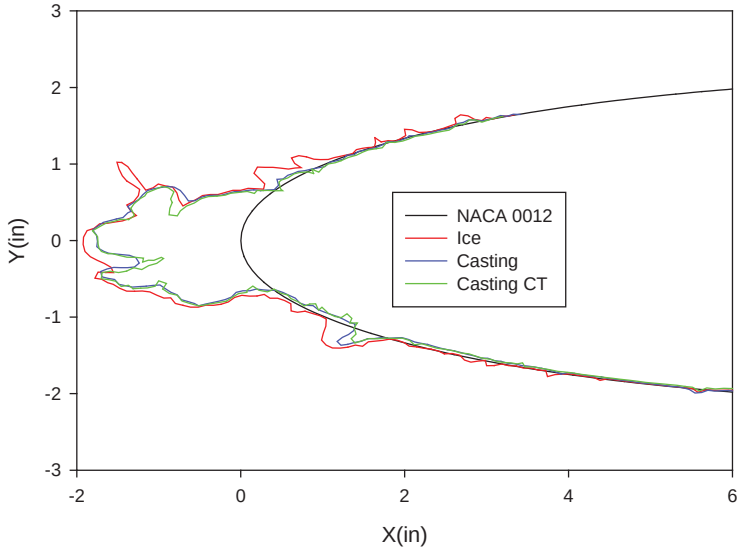

b) Cross sectional cuts

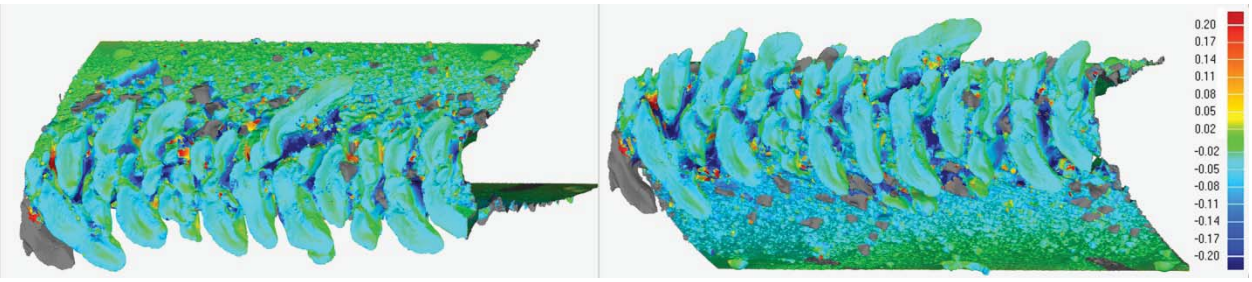

c) Deviation map of cast ice shape compared to ice scan (Left: upper surface, Right: lower surface)

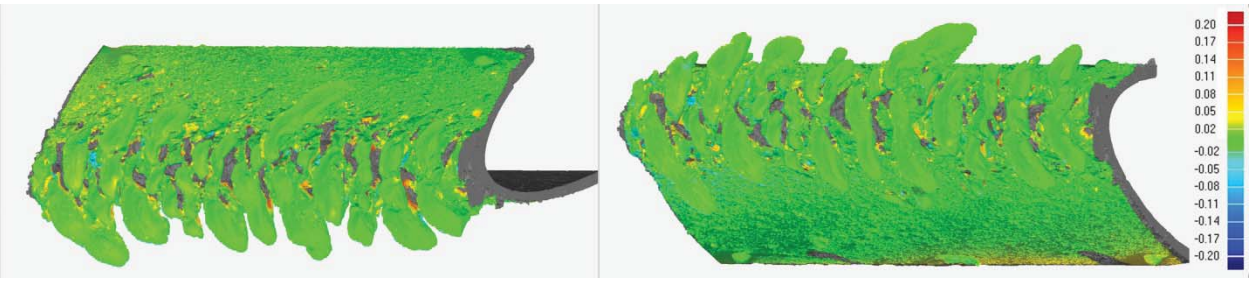

d) Deviation map of cast ice shape compared to CT scan (Left: upper surface, Right: lower surface)

Figure 31 Complete scallop ice scan/casting comparison (AF2037).

B. Run AF2032-Incomplete Scallop Ice Accretion

Figure 32 shows the results from run AF2032, which was an incomplete scallop ice accretion. Figure 32b shows the 2-D cross sectional cuts of the scanned ice accretion and the cast ice shape at the centerline of the tunnel. The scan of the casting was smaller when compared to the original ice accretion scan, indicating that it had shrunk during the mold/casting process. There were numerous gray areas in the deviation map due to scallops and feathers

that were present in the original ice scan, but not in the casting. Again, these were features that broke off during the casting process.

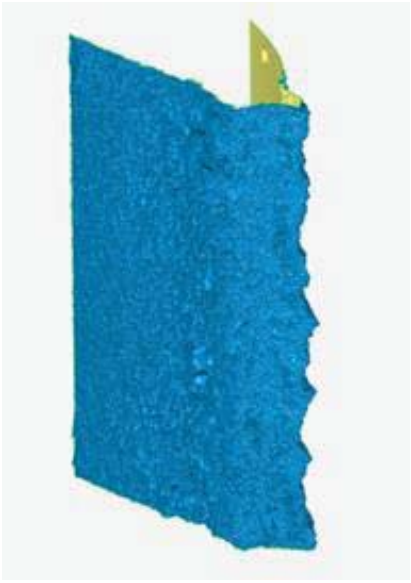

a) Water-tight scan

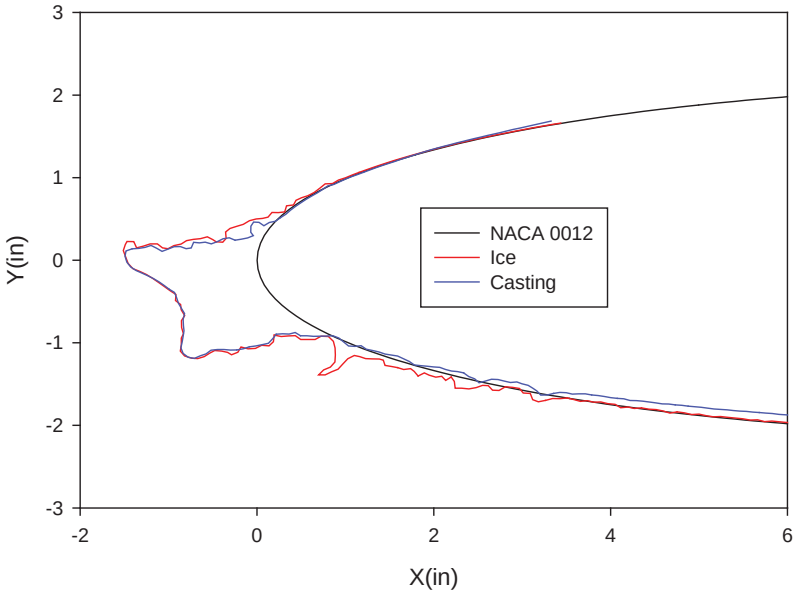

b) Cross sectional cuts

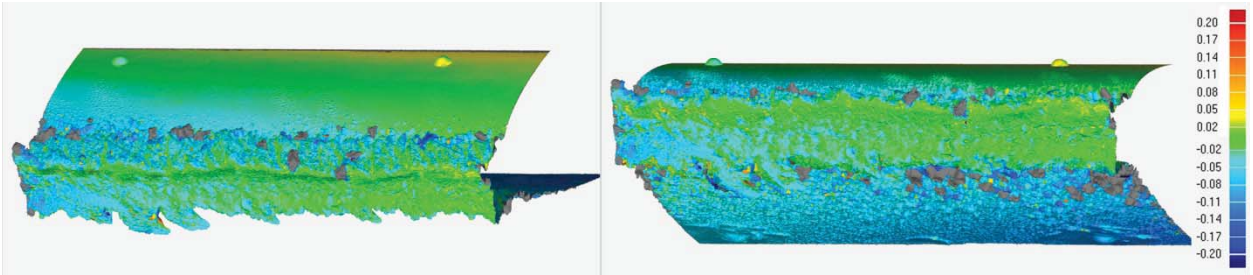

c) Deviation map of cast ice shape (Left: upper surface, Right: lower surface)

Figure 32 Incomplete scallop ice scan/casting comparison (AF2032).

C. Run AF2029-Roughness Ice Accretion

Figure 33 shows the results from the run AF2029, which was a roughness ice accretion. Figure 33b shows the 2-D cross sectional cuts of the scanned ice accretion and the cast ice shape at the centerline of the tunnel. The scan of the casting was smaller when compared to the original ice accretion scan, indicating that it had shrunk during the mold/casting process.

a) Water-tight scan

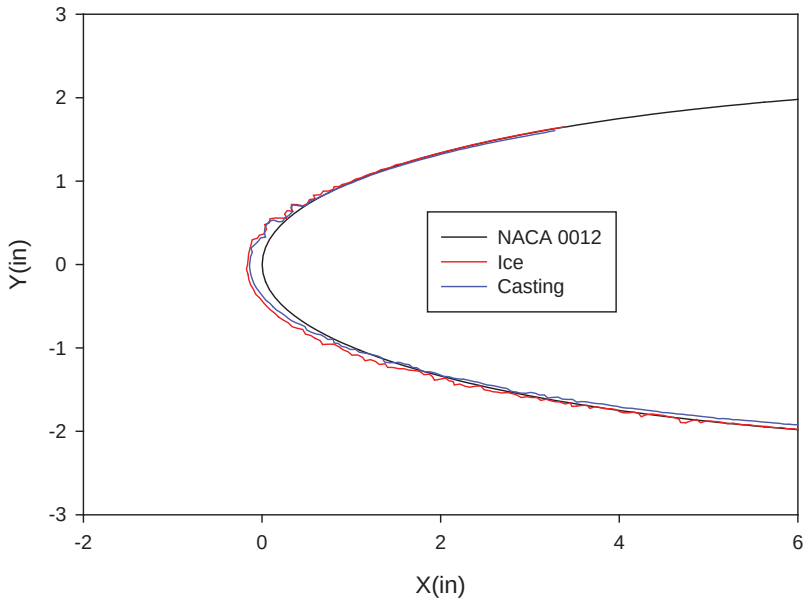

b) Cross sectional cuts

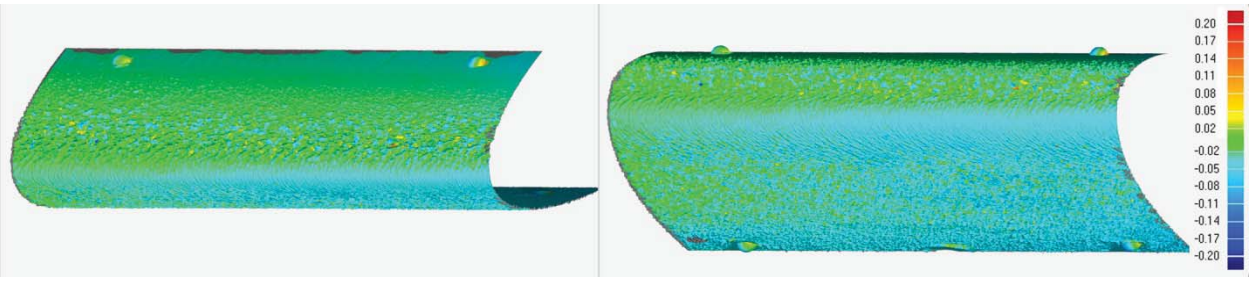

c) Deviation map of cast ice shape (Left: upper surface, Right: lower surface)

Figure 33 Roughness ice scan/casting comparison (Run AF2029).

D. Run AF2032-Rime Ice Accretion

Figure 34 shows the results from the run AF2032, which was a rime ice accretion. Figure 32b shows the 2-D cross sectional cuts of the scanned ice accretion and the cast ice shape at the centerline of the tunnel. The scan of the casting was smaller when compared to the original ice accretion scan, indicating that it had shrunk during the mold/casting process. There were numerous gray areas in the deviation map due to scallops and feathers that broke off during the casting process.

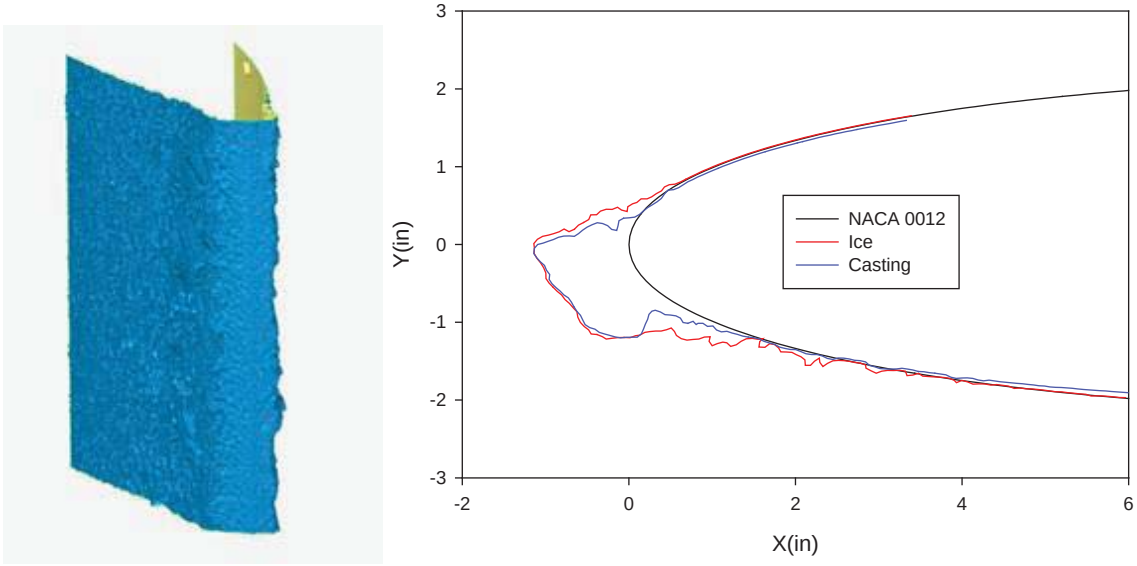

a) Water-tight scan **b) Cross sectional cuts**

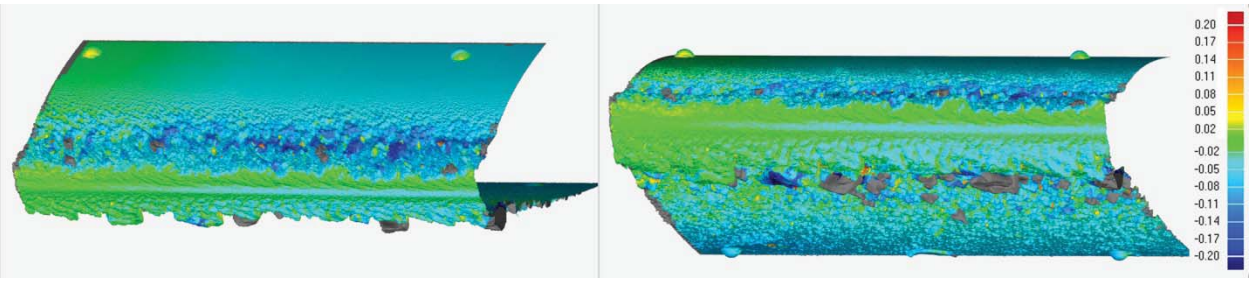

c) Deviation map of cast ice shape (Left: upper surface, Right: lower surface)

Figure 34 Rime ice scan/casting comparison (Run AF2028).

E. 3-D Swept Wing Ice Comparison Summary

The results from geometric comparisons on the swept wing showed that most of the relevant features of an ice shape could be measured with the laser scanning method. Significant portions of the scallop features were captured with the laser scanner and the results compared very well with the CT scanning methods, except for the deep gaps between the scallops. It is currently not known how aerodynamically important these deep gap regions are. Further aerodynamic studies would be required to make such an assessment.

As with the results from the straight wing tests, the cast shapes appeared to have shrunk and warped during the curing process, and it was difficult to precisely align the scans of the casting to the scans of the original ice accretion. This was further compounded by missing scallop and feather features on the cast shapes that broke off during the mold/casting process.

VII. Conclusions

A research program has been implemented to develop and validate the use of a commercial 3-D laser scanning system to record ice accretion geometry in the NASA Icing Research Tunnel. Phase I of the research effort was conducted to identify the most suitable laser scanning hardware and software for further development. Phase II of the research effort was to implement the system and validate its capability to geometrically record the aerodynamically relevant features.

The results of Phase I showed that commercial 3-D laser scanners were capable of recording many details of various types of ice shapes, and post-processing software were capable of generating "water-tight" surfaces. Several scanning systems were evaluated against selection criteria, and an arm-based system was found to be the most promising. In Phase II, this scanner system was used to implement and validate the use of this technology through a series of icing and aerodynamic tunnel tests.

The results from geometric comparisons on the straight wing showed that the ice shape models generated through the scan/RPM process compared reasonably well with the cast shapes. It was difficult to precisely compare the scans of the cast shapes to the original ice accretion scans because the cast shapes appear to have shrunk during the mold/casting process by as much as 0.10-inch for the glaze-horn cast shape. However, the comparison of the local ice shape features was possible and produced better results. The RPM manufacturing process was shown to reproduce the original ice accretion scan normally within 0.01-inch.

The results from geometric comparisons on the swept wing showed that most of the relevant features of an ice accretion could be measured with the laser scanning method. Significant portions of the scallop features were captured with the laser scanner, and the results compared very well with the CT scanning methods, except for the deep gaps between the scallops. It is currently not known how aerodynamically important these deep gap regions are, and aerodynamic studies would be required to make such an assessment.

As with the results from the straight wing tests, the cast shapes from the swept wing appeared to have shrunk and warped during the curing process, and it was difficult to align the scans of the casting to the scans of the original ice accretion. This was further compounded by missing scallop and feather features on the cast shapes that broke off during the mold/casting process.

Phase II of this study is now complete. A method to accurately and efficiently digitize ice accretions in three dimensions is now available. In the process of implementing and validating the laser-based scanning system, some limitations in its capabilities have been identified. However, the laser-scanning method (with its high level of resolution and accuracy) also identified limitations in the traditional mold/casting method (which has been used as the benchmark 3-D ice documentation method for years). The laser-scanning method can now be used to increase the utility of icing wind-tunnel tests by improving the documentation of ice accretions.

Acknowledgements

This work was funded by NASA Atmospheric Environment Safety Technologies Project. The authors would like to thank the Icing Research Tunnel personnel, Paul Tsao, Robert Sills, and Jonathan Herman for their contributions during the IRT test and post-processing of the data. Special thanks goes to Brian Brandenburg at NASA and Dave Foley at University of Illinois for the manufacture of the cast ice shapes used in this study.

References

[1] Broeren, A.P., Addy, H.E., Jr., Bragg, M.B., Busch, G.T., Guffond, D., and Montreuil, E., "Aerodynamic Simulation of Ice Accretion on Airfoils," NASA/TP—2011-216929, June 2011.

[2] Reehorst, A.L. and Richter, G.P., "New Methods and Materials for Molding and Casting Ice Formations," NASA TM 100126, Sept. 1987.

[3] Colantonio, R., "Atmospheric Environment Safety Technologies (AEST) Project Overview," NASA Aviation Safety Program Annual Technical Meeting, St. Louis, MO, May 10-12, 2011.

[4] Potapczuk, M., "Airframe Icing Technical Challenge," NASA Aviation Safety Program Annual Technical Meeting, St. Louis, MO, May 10-12, 2011.

[5] Lee, S., "Status of 3D Ice Shape Measurement Effort," NASA Aviation Safety Program Annual Technical Meeting, St. Louis, MO, May 10-12, 2011.

[6] Lee, S., Broeren, A.P., Addy., H.E., Sills, R., and Pifer, E., "Development of 3D Ice Accretion Measurement Method," 4th AIAA Atmospheric and Space Environments Conference, New Orleans, LA, June 25-28, 2012, AIAA Paper 2012-2938

[7] Kreeger, R.E. and Tsao, J., "Ice Shapes on a Tail Rotor," AIAA 6th Atmospheric and Space Environments Conference, Atlanta, GA, June 16-20, 2014, (Submitted for publication).

[8] McClain, S.T., Reed, D., Vargas, M., Kreeger, R.E., and Tsao., J.C., "Ice Roughness in Short Duration SLD Icing Events," AIAA 6th Atmospheric and Space Environments Conference, Atlanta, GA, June 16-20, 2014, (Submitted for publication).

[9] http://hexagonmetrology.us.

[10] http://www.geomagic.com.

[11] Broughton, H., "3D Laser Scanner Project," Subcontract No. 011422 Report, Feb. 2004.

[12] Broeren, AP, Addy, H.E., Lee, S., and Monastero, M.C., "Validation of 3-D Ice Accretion Measurement Methodology for Experimental Aerodynamic Simulation," AIAA 6th Atmospheric and Space Environments Conference, Atlanta, GA, June 16-20, 2014, (Submitted for publication).

[13] Monastero, M.C., "Validation of 3-D Ice Accretion Documentation and Replication Method Including Pressure-Sensitive Paint," M.S. Thesis, Dept. of Aerospace Engineering, Univ. of Illinois at Urbana-Champaign, 2013.

[14] Vargas, M. and Reshotko, E., "Physical Mechanisms of Glaze Ice Scallop Formations on Swept Wings," NASA TM-1998-206616, *AIAA* Paper 98-0491, January 1998.